NASA Technical Paper 3045

December 1990

A Method for the Design of Transonic Flexible Wings

Leigh Ann Smith
and Richard L. Campbell

NASA

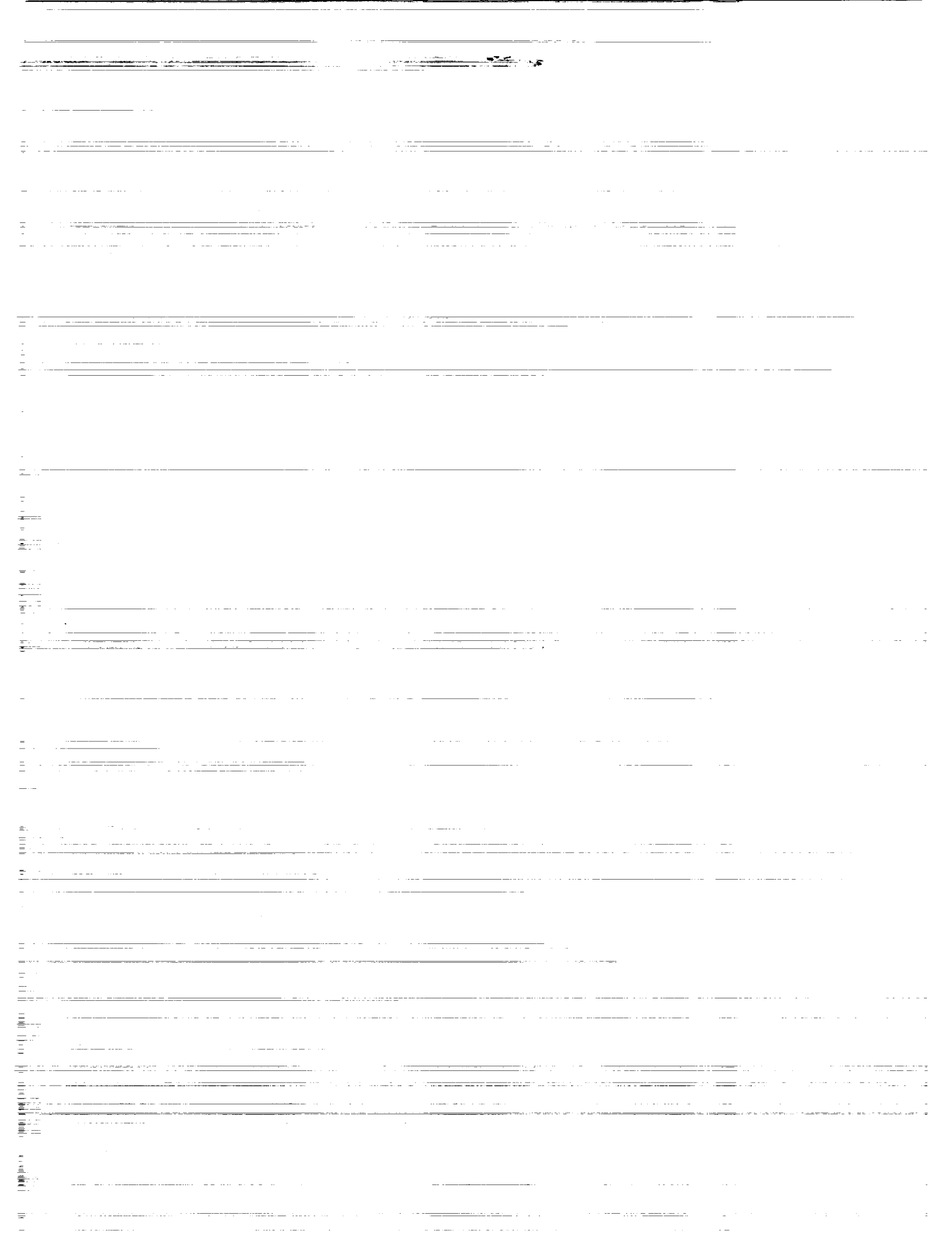

NASA Technical Paper 3045

1990

A Method for the Design of Transonic Flexible Wings

Leigh Ann Smith
and Richard L. Campbell
Langley Research Center
Hampton, Virginia

National Aeronautics and Space Administration
Office of Management
Scientific and Technical Information Division

Summary

Methodology has been developed for designing transonic airfoils and wings; it includes a technique that can account for static aeroelastic deflections. This procedure is capable of designing either supercritical or more conventional airfoil sections. Methods for including viscous effects are also illustrated and are shown to give accurate results.

The methodology developed is an interactive system containing three major parts. A design module has been developed that modifies airfoil sections to achieve a desired pressure distribution. This design module works in conjunction with an aerodynamic analysis module, which for this study is a small perturbation transonic flow code. Additionally, an aeroelastic module is included that determines the wing deformation due to the calculated aerodynamic loads. Because of the modular nature of the method, it can be easily coupled with any aerodynamic analysis code.

Test cases are shown to demonstrate the viability of the method. The designs obtained generally match the target pressures and the airfoils used to generate them. For supercritical airfoil sections, the shock locations and the cusp regions were accurately reproduced by the method; however, some small discrepancies are noted near the leading edge. These differences are caused by the smoothing method chosen, and ways of eliminating them are discussed.

Additionally, a case is shown that demonstrates use of the method to produce an entirely new design from an arbitrary target pressure distribution. This study found target pressure generation to be the most crucial step in the design process.

Introduction

A considerable amount of development work has been done in the area of transonic wing design. At present there is a wide spectrum of design codes available, each with its own strengths and weaknesses. Each method is unique in some way, which makes grouping them difficult. The following paragraphs address some of the most often quoted classifications.

One of the earliest design procedures, often classified by itself, is the hodograph method by Bauer et al. (1972). This technique uses a variable transformation to the hodograph plane which linearizes the partial differential equations for compressible potential flow.

Direct methods are another class of design approach. These methods are characterized by a direct analysis on a wing or airfoil. A procedure is used to modify the shape, which is then analyzed directly to determine its new performance characteristics. Through several iterations of design estimates and performance predictions, a final design with the required performance is found. Often this process is automated, so that new design modifications are made by computer for each cycle.

Shortly after the hodograph method was introduced, Barger and Brooks (1974) published a design method based on streamline curvature. Their method of modification alters the airfoil to produce a pressure distribution that, with each iteration, more closely matches a specified target distribution. Davis (1979) has also published a direct method, which is an automated extension of the work by Barger and Brooks (1974).

Optimization methods are also considered to be direct methods. They try to minimize a certain function, such as drag, by modifying and analyzing a design shape. Hicks, Murman, and Vanderplaats (1974) developed one of the first optimization methods for airfoil design based on Vanderplaats' (1973) optimization module, CONMIN. CONMIN continues to be widely used today. Kennelly (1983) has developed an airfoil design code using a quasi-Newtonian optimization method, QNMDIF. This method was shown to be more reliable and efficient than the conjugate-gradient method used in CONMIN.

Inverse methods depend on a formulation of the design problem that starts with a desired (target) surface pressure distribution and then determines the airfoil shape that would have produced it. The target pressures are used to determine velocities along the airfoil surface. These velocities are the boundary conditions for the flow field solution. After each iteration, the surface on which these boundary conditions are applied is changed in an attempt to reduce the normal component of velocity. When the normal component of velocity is zero, the surface is the proper airfoil shape. Unfortunately, the airfoil surfaces derived may cross or leave an open trailing edge. One of the first transonic inverse methods was developed by Tranen (1974). Volpe and Melnik (1985) have formulated the first correctly posed inverse method for two-dimensional flow. Their technique eliminates the problem of trailing-edge closure.

Sobieczky et al. (1979) introduced the fictitious gas method. This formulation designs an airfoil that will yield shock-free flow at a given Mach number and angle of attack. His method alters the density of the gas in supersonic regions so that the flow equations remain elliptic. Then the supersonic region is recomputed from the potentials along the sonic line. The airfoil surface is altered to conform to a streamline through this supersonic zone.

More sophisticated analysis codes have brought many improvements to the early methods of airfoil design cited above. Many have been extended to include three-dimensional wings and viscous effects. Although many computational techniques now exist for the automated design of transonic wings, a literature search shows that currently there are no published methods that consider the effects of aeroelasticity. Deformation due to loads encountered in flight can have a significant effect on the performance of a wing by changing the local surface angle of attack, which causes a change in lift distribution. The procedure described in this document is the result of an effort to develop a methodology for transonic wing design that takes aeroelastic considerations into account.

For this project, a direct method was developed that is similar to the work of Barger and Brooks (1974) and Davis (1979). The method is coupled with a small perturbation code to aerodynamically analyze complex configurations and with an aeroelastic module to include the effects of wing deflections on the performance of the configuration.

A means of accounting for viscous effects is also included for use with the current method. Supercritical airfoil sections are especially subject to the decambering effects of a boundary layer, which can cause a significant lift loss at transonic speeds.

Symbols

b	wingspan
c	local chord
c_{ave}	average chord
$c_i,\ i = 1,5$	smoothing equation coefficients
c_l	section lift coefficient
C_L	wing-body lift coefficient
C_P	pressure coefficient
C_P^*	local sonic pressure coefficient
M	Mach number
R	Reynolds number based on chord
x	streamwise coordinate
y	height coordinate
α	angle of attack
η	spanwise location, $2y/b$

Description of Design Method

Overview of Method

A flowchart of the design procedure is shown in figure 1. The design method begins with the input of a starting shape and flow parameters to the aerodynamic analysis module. The shape information may include a single airfoil shape for a two-dimensional case, or a planform shape and airfoil sections for a wing. The aerodynamic analysis module is a transonic small disturbance analysis code that employs an iterative solution procedure. Initially, several iterations of the procedure are performed to obtain a rough estimate of the flow field. When the aerodynamic analysis has completed a preset number of iterations through the solution, the method transfers control to the design module. This module redefines the shape of the airfoils based on the difference between the current analysis and the target pressure distribution. This completes one design cycle.

Each design cycle yields a modified airfoil or wing. The new shape is input to the aerodynamic analysis module where more iterations of the solution, usually about 25, are performed before returning to the design module for a new shape correction. The process is then repeated for a number of design cycles set by the user.

Aeroelastic effects may be determined interactively, in conjunction with the design, or determined after the design is completed. When the interactive approach is chosen, the design method transfers control to the aeroelastic module after every 20th iteration through the solution process of the aerodynamic analysis module (fig. 1(a)). The aeroelastic module determines the wing deflections and sends the deformed wing shape back to the aerodynamic analysis module to be analyzed for 20 more iterations. This pattern allows at least one aeroelastic update to the analysis before each design shape is computed. Since the changes computed for each design cycle are relatively small, 20 iterations between aeroelastic calculations is more than sufficient. When aeroelastic effects are determined in the postprocessing mode, the aeroelastic module determines wing deflections once, after all other calculations have been completed (fig. 1(b)).

Viscous effects can also be considered when using this design method. When the aerodynamic analysis module includes a boundary-layer calculation, it can be used interactively during the design process. Alternately, a boundary-layer thickness can be determined by postprocessing, and subtracted from the design.

It is important to note that the success of the design method is not dependent on the choice of aerodynamic analysis module. The wing-body-pod-pylon-winglet (WBPPW) transonic small disturbance code by Boppe (1987) was chosen for this exercise because

of its speed and ability to handle complex configurations, but the design method can be coupled with any aerodynamic analysis code.

Design Algorithm

The design algorithm employed was developed by Campbell and Smith (1987). It compares pressures computed by the analysis module with a target pressure distribution and computes a modification to the airfoil section or sections. For three-dimensional cases, analysis pressures at the computational stations are interpolated to the input locations and compared point by point with the input target pressures to determine the changes needed. The algorithm relates changes in surface pressure coefficient to changes in surface curvatures or slope, depending on local velocities.

The algorithm originated with the observation from analyses of airfoils that changes in airfoil surface curvature generally gave proportional changes in the pressure coefficients. This relationship can be derived from the momentum equation in streamline curvature form,

$$dq/q = -C(n)\ dn \tag{1}$$

where q is the local velocity, C is the streamline curvature, and n is the direction normal to the streamlines. Following the analysis of Barger and Brooks (1974), the distribution of curvature normal to the streamlines is assumed to be

$$C(n) = C_0\ e^{-kn} \tag{2}$$

where k is a constant and the subscript 0 denotes the value at the airfoil surface. For positive values of k, this expression yields the correct values of C_0 and zero for the streamline curvature at the airfoil surface and in the far field, respectively. Substituting this expression into the momentum equation and integrating gives

$$C_0 = k\ \ln(q_0/q_\infty) \tag{3}$$

where the subscript ∞ indicates the free-stream value. If small changes in velocity are assumed the equation becomes

$$\Delta\ C_0 = k\ \Delta q_0/q_0 \tag{4}$$

Barger and Brooks (1974) suggest letting k be proportional to C_0, which yields the following relationship between surface curvature and velocity:

$$\Delta C = A_1 C\ \Delta q/q \tag{5}$$

where A_1 is a constant, and the zero subscripts have been dropped for simplicity. If small-disturbance assumptions are made ($\Delta q = \Delta u$, $q = q_\infty$, $C_P = -2u/q_\infty$, where u is the perturbation velocity in the free-stream direction and C_P is the pressure coefficient), equation (5) becomes

$$\Delta C = AC\ \Delta C_P \tag{6}$$

where $A = -0.5A_1$. In the above equation, as C approaches zero, a small change in curvature would result in a very large change in pressure coefficient. This does not occur in actual cases and probably results from the assumed normal curvatures distribution used in integrating the momentum equation. The curvature term has therefore been replaced with the following:

$$(1 + C^2)^B \tag{7}$$

where B is an input constant ranging from 0.0 to 0.5. This term approaches a value of 1.0 for small values of curvature, giving equation (6) the form

$$\Delta C = A\ \Delta C_P \tag{8}$$

For small values of surface slope where the curvature is approximately equal to the second derivative of the airfoil ordinate in the streamwise direction (y''), equation (8) is proportional to the expression given by Davis (1979), converted to incremental form, for subsonic flow past a wavy wall

$$\Delta y'' = k\ \Delta C_P \tag{9}$$

where k is a constant. For the larger values of curvature encountered in the nose region, the curvature term approaches C^{2B}. The value of B is reduced for cases with supercritical flow to help stabilize the solution. The final equation is therefore

$$\Delta C = \Delta C_P\ A(1 + C^2)^B \tag{10}$$

with the sign of A reversing for the lower surface.

While this algorithm works for both subsonic and transonic cases, it was found to converge rather slowly when strongly supercritical flow (local Mach number greater than about 1.15) was present. As pointed out by Davis (1979), the relationship of pressure coefficient and airfoil geometry would be expected to change character as the flow becomes locally supersonic. A hybrid algorithm similar in concept to Davis' was therefore developed based on supersonic thin airfoil theory. The equation for the

pressure coefficient is given in Liepmann and Roshko (1957) as

$$C_P = 2y' \Big/ \sqrt{M_\infty^2 - 1} = k_1 y' \qquad (11)$$

where y' is the surface slope. This can be rearranged to yield

$$\Delta y' = k\ \Delta C_P \qquad (12)$$

for increments in C_P and y'. Differentiating this expression with respect to x gives

$$\Delta y'' = k \frac{d}{dx}(\Delta C_P) \qquad (13)$$

Since the thin airfoil equation is strictly valid only for supersonic free-stream Mach numbers, an equivalent value for k must be determined. If the free-stream Mach number in equation (11) is replaced with the switching Mach number of 1.15, the value of k would be 0.28. In order to underrelax the changes in geometry, a value of 0.05 was used with good results. Several switching Mach numbers were also tried in various test cases. It was found that using the supersonic formula when the local Mach number just reached 1.0 adversely affected the design process. Apparently the supersonic character of the flow is not established until local Mach numbers of about 1.15–1.20 are present.

The hybrid algorithm is implemented by using the surface curvature relation for regions without strongly supercritical flow and a combination of the surface curvature and supersonic approaches in the higher Mach number regions. In order to modify the airfoil, changes in curvature are first converted to changes in y'' using the formula

$$\Delta y'' = \Delta C \left[1 + (y')^2\right]^{1.5} \qquad (14)$$

which assumes that the surface slope does not change appreciably. A change in y'' at a single point can be made as shown in figure 2. To increase the magnitude of y'' at point I without changing y'' at the other locations, points $I + 1$ though N are sheared through a given angle. After all the points are modified as desired, the entire surface is rotated about the leading edge so that a given trailing-edge thickness is maintained (fig. 2(b)). This is important since crossed or open trailing edges could result if the leading-edge design is just slightly in error. This final rotation slightly changes the new values of curvature, but the changes are negligible as the solution approaches convergence. Because the method is applied point by point, a user can specify a particular region of an airfoil to be modified without disturbing the rest of the airfoil shape.

The design algorithm is applied in the same manner whether the case is two- or three-dimensional. For a wing, the design modifications are determined and applied to each input section individually. The results of test cases have shown this approach to be satisfactory.

Smoothing the airfoil section surfaces is found to be necessary to obtain a converged design solution for most cases. After the airfoil section is modified in each design cycle, the coordinates are smoothed by fitting them piecewise to two polynomials, one for the leading edge and a second for the remainder of the airfoil. Over most of the airfoil (aft of 20 percent chord), a third-order polynomial is used,

$$y = c_1 + c_2 x + c_3 x^2 + c_4 x^3 \qquad (15)$$

with a least-squares fit. Sets of seven consecutive points along the airfoil surface are used to obtain the fit. Three points on either side of the center point determine the coefficients of the polynomial, and a new value is computed for the center point. Near the leading and trailing edges, the point to be adjusted may not fall in the center of the seven points. The leading- and trailing-edge points remain fixed, and the points near them are adjusted by fitting the curve through the nearest six points. The scheme is applied from the leading to the trailing edge so that all the points except the first and last are adjusted.

In the leading-edge region, a third-order polynomial does not yield the best fit to the airfoil section; a square root term must be added to the polynomial to give the proper curvatures. This five-term equation

$$y = c_1 + c_2 x + c_3 x^2 + c_4 x^3 + c_5 x^{0.5} \qquad (16)$$

can be unstable and cause a design to diverge when large changes to the airfoil section are required. Dropping the second- and third-order terms from equation (16) yields the three-term equation

$$y = c_1 + c_2 x + c_5 x^{0.5} \qquad (17)$$

which improves the stability of the design method but can cause discrepancies between the design and target pressures. This effect is illustrated in test cases described later in this report.

A procedure similar to the smoothing method is used to allow airfoil sections to rotate automatically during the design process. A rotation procedure is needed because the design algorithm is constrained to make its changes without moving the first and last points on each airfoil surface. As a consequence,

when angle-of-attack changes are needed in a design, the leading-edge curvature of one surface increases while the other decreases, resulting in a redistribution of airfoil thickness, especially near the leading edge. Thus, the new camber or midthickness line will lie above or below the previous one, but will still be constrained to pass through the leading-edge point. By using the new camber line to extrapolate a curve through the leading-edge area, the airfoil coordinates can be adjusted in this area, and the section can be allowed to rotate (fig. 3(a)).

In this procedure, the camber line coordinates are computed for all the input values of x/c in the leading-edge area, back to the sixth input point aft of $x/c = 0.02$. These last six camber line points are used to determine coefficients for a cubic polynomial curve fit through the points. The points ahead of $x/c = 0.02$, including the first point, are adjusted to lie on this curve. This adjustment is then applied to the corresponding airfoil coordinates to slightly reshape the leading edge (fig. 3(b)). Because the rotation changes are introduced to the procedure as small geometric changes, it is ensured that design changes to the surface curvature keep pace with the rotation changes and the design proceeds in a controlled fashion.

Aerodynamic Analysis

The wing-body-pod-pylon-winglet transonic small disturbance code (WBPPW) by Boppe (1987) was chosen as the aerodynamic analysis module for this study. It has the capability of modeling complex three-dimensional aircraft geometries with associated pods, pylons, and winglets, as well as two-dimensional airfoils, at transonic speeds. The code has been used successfully for a wide range of configurations. A two-dimensional strip boundary-layer approximation based on the method of Bradshaw and Ferriss (1971) is included.

WBPPW uses two Cartesian grid systems in its solutions. The flow field is initially solved in a global crude grid system that encompasses the entire flow field. Embedded fine grids are used in areas of interest where flow field gradients may be large, such as near the wing and the fuselage. After the initial iterations have been computed on the crude grid, solutions are obtained on the fine grid, using the values at the crude grid points as Dirichlet boundary conditions on the outer boundaries of the fine grids. Then the crude grid values are recomputed, using the fine grid values as Neumann boundary conditions on the configuration surface. One pass through each of the two grid systems represents one aerodynamic iteration. A discussion of convergence considerations is included in the appendix.

Structural Analysis

The Transonic Aeroelastic Program System (TAPS) (Campbell, 1984) is used in conjunction with the aerodynamic analysis code and design module to complete the aeroelastic design method. It can be used interactively or in a postprocessing mode. The TAPS portion of the method determines the deformation of the wing shape under the current load. In the interactive mode that information is sent to the aerodynamic analysis code and updated after every 20 crude/fine aerodynamic analysis iterations. In the postprocessing mode the deformation information is applied only to the final design.

To use the TAPS module, a flexibility influence coefficient matrix must first be obtained for the wing structure. This matrix may be determined computationally or experimentally. The coefficients produced are obtained by choosing "nodes" or points on the wing surface and then determining the vertical deflection of each node when a unit normal force is applied individually at each of the other nodes on the wing. This results in a square matrix containing, for every node, a deflection due to a unit force at each of the other nodes. In the TAPS module, the computed wing pressures are interpolated to the node locations and assumed to act uniformly over an area associated with each node. This area surrounds the node and is a quadrilateral whose edges lie half way between the current node and surrounding nodes. A force and a resulting deflection are then computed at each node location. These deflections are used to update the surface slopes, which serve as boundary conditions in the aerodynamic module.

Results and Discussion

Test cases have been performed to evaluate the accuracy of the design method. Several of them are discussed below. These cases demonstrate use of the procedure on supercritical airfoils and wings and show methods of including viscous and aeroelastic effects in the design process. Also, an applications case is presented, in which a new wing is designed from an arbitrary pressure distribution.

All the test cases presented below were obtained using a standard procedure, with some variations for viscous or aeroelastic effects. The first step in preparing a test case is to generate a set of target pressures. In all but the applications case, these pressures were generated by analyzing a known airfoil or wing with the WBPPW analysis code. Since the design method uses the same flow solver, differences between the design computation output and the original targets can be attributed to the design method rather than the accuracy of the aerodynamic analysis

procedures. After the target pressures were generated, a NACA 0006 airfoil section was used as a starting airfoil and modified by the design method until it produced the target pressure distribution. Because large changes in the section shape were anticipated, the three-term equation (17) was used in the smoothing procedure. The results obtained are discussed below. For uniformity, all cases were allowed to iterate for 90 design cycles. Some of the cases converged more quickly, but 90 cycles have been found to be sufficient for almost all cases and are not prohibitively expensive. Solution convergence is discussed in more detail in the appendix.

Supercritical Airfoil With Viscous Effects

The first set of test cases illustrates use of the method to design a supercritical airfoil and shows methods for including viscous effects in the computation. Viscosity can have a significant effect on the performance of a supercritical airfoil at transonic speeds because of the decambering effect of the boundary layer. Figure 4 illustrates this by showing two analyses of the same airfoil, one with viscous effects included and one without. While there is little difference in the pressures corresponding to the forward region of the airfoil where the boundary layer is thin, further aft there is a large difference in shock location, as well as in the compression in the lower surface cusp region, and the viscous case obviously has much less lift. To ensure that an airfoil design will have the desired performance, one should account for viscous effects in the design procedure.

Two procedures for including viscous effects are outlined in the following discussion. The first case determines viscous effects interactively, and the second uses a postprocessing method.

Interactive boundary layer. The first approach to viscous design is to utilize the interactive boundary-layer capability of the aerodynamic analysis code to couple the viscous and inviscid analyses during the design process. This allows the code to compute a boundary-layer thickness, apply it to the airfoil design, and have its effect included in the pressure calculations for each aerodynamic iteration.

A section from the aeroelastic research wing ARW-2 (Seidel et al., 1985) was used in illustrating this method. This wing is fully described below with the three-dimensional cases. The section was analyzed at Mach 0.77, an angle of attack of 1°, and a Reynolds number of 5 million to generate target pressures. Viscous effects were included in the analysis. Then a design run was made, with the boundary layer being updated interactively during the design process.

The results of this case are presented in figure 5. Figure 5(a) shows the target pressure distribution from the viscous analysis of the original supercritical airfoil shape (target) as well as the pressure distribution from the final cycle of the inviscid design run (final). Also included is the pressure distribution computed from a viscous analysis of the designed shape (analysis).

While the three distributions shown agree over most of the airfoil, the leading-edge pressures for the final and analysis computations are slightly different from the target pressures in that region. This discrepancy is a result of using the three-term equation (17) in the smoothing procedure, as is illustrated in the section on smoothing considerations below.

The resultant airfoil shape is shown in figure 5(b). It is compared with the original section used to generate the targets. Note that the vertical scale is expanded to show detail. While there is a slight discrepancy in thickness, the overall shape and curvature appear to match very well. Too much curvature at some point on the leading edge of the lower surface causes the discrepancy seen on the lower surface. Also, a difference in the size of the trailing-edge thickness for the starting and target airfoils accounts for some of the discrepancy.

It should be noted in this case and the following ones that the airfoil coordinates labeled "target" only define the shape used to generate the target pressures. It is expected that to reach the target pressures the design will need to replicate this shape; however, the design is in no way restricted to this shape.

Postprocessing boundary layer. The approach used in the postprocessing procedure is to compute the displacement thickness in advance and include it as part of the airfoil shape in an inviscid design computation. This method requires several steps. First, a target pressure distribution must be determined that includes viscous effects. From this target pressure distribution, the boundary-layer thickness is evaluated. To ensure sufficient trailing-edge thickness, the boundary-layer thickness is added to the initial airfoil prior to the start of the design process.

Once the initial shape has been determined, an inviscid design computation can be made. The airfoil generated by the design process will then include the thickness of the boundary layer and will need to be reduced by that amount to complete the design. This method requires less computer time than the previously described method and may be more robust, as the sudden changes in thickness associated with boundary-layer development are eliminated.

The target pressures from the previous case were used for this design run. An estimate of the boundary-layer thickness was made from the target pressures by using the method of Bradshaw and Ferriss (1971), which is part of the aerodynamic analysis code. This boundary-layer thickness was then added to the initial airfoil, a NACA 0006, to ensure sufficient thickness at the trailing edge. This initial shape was input to the design method, and an inviscid design computation was performed. The airfoil generated by the last design cycle was saved, and the previously computed boundary-layer thickness was subtracted from it. The resultant airfoil is the completed design shape.

The results are shown in figure 6. Figure 6(a) shows the discrepancy in the leading-edge region due to smoothing as seen in the previous case. Additionally, the analysis curve shows the shock to be slightly smeared, and the last 20 percent of the analysis curve shows additional small deviations. Since these discrepancies are not present in the interactive case, they must be attributable to the boundary-layer thickness calculation. The computed boundary layer has spikes of high negative curvature in the shock and trailing-edge areas. When these areas are subtracted from the smooth inviscid design, the resulting airfoil is not smooth. Several attempts were made at improving the correlation by smoothing the airfoil, but this was found to change the character of the airfoil in the process of eliminating the curvature spikes.

Figure 6(b) shows the final design airfoil after the boundary-layer thickness has been subtracted from its upper and lower surfaces. This shape is not substantially different from the interactive boundary-layer method design. Again the lower surface curvature has made the airfoil thinner than the original shape. Despite these small discrepancies, the results indicate that this is a viable method of accounting for viscous effects.

This case required 166 seconds of cpu time on the NASA Langley Cray-2 computer for the inviscid design portion. For the previous case, 220 seconds were required. The time penalty is probably outweighed by the simplicity and accuracy of the interactive method.

Interactive boundary layer with automatic twisting. The development of the automatic twisting procedure allowed its use in the third approach to this design case. Since the automatic twisting procedure allows the leading-edge points to be changed, the curvatures in the leading-edge region are not as constrained as in the previous two cases. The interactive boundary layer was also used for this case.

In figure 7(a), the pressure distributions are shown to be well matched. There is a slight discrepancy near the trailing edge for the analysis run. Figure 7(b) shows a very good comparison to the original airfoil. The thickness is well matched between the target and final airfoils. The only discrepancy is again in the trailing-edge area where the trailing-edge thickness is constrained to be slightly different for the two airfoils.

Smoothing considerations. In each of the previous cases, a discrepancy in the leading-edge region has been attributed to using the three-term equation (17) in the smoothing method. To demonstrate this effect, the previous case was repeated using the five-term equation (16) in the leading-edge region. The results are shown in figure 8. The automatic twist procedure increases the stability of the five-term smoothing procedure; however, more design cycles are required to obtain a converged solution. This case required an additional 40 cycles.

The pressure plot shows that the five-term smoothing method has eliminated the discrepancy in the leading-edge region seen in the three-term case. However, downstream the shock region match has been disturbed. Comparing figures 7(b) and 8(b) shows no significant difference between this airfoil and the one computed for the previous case. Again the trailing-edge thickness causes the aft portion of the airfoil to be slightly displaced from the targets.

Plotting the surface curvatures of the original airfoil shows that the target section itself is not smooth. This could contribute to the discrepancies noted above, namely that the smooth design airfoil does not and can not match the original, rough airfoil. To test this theory, an additional design case was performed, this time smoothing the target airfoil shape before generating a new set of target pressures at similar conditions. Also for this case, the starting NACA 0006 airfoil surfaces were sheared slightly to increase the trailing-edge thickness to that of the design, eliminating any discrepancies due to that difference. Five-term smoothing is used to obtain the best match in the leading-edge region. The results of this case are shown in figure 9.

The results of this case show the best agreement between design and target of all the cases in this section. The final design pressures pass through all the target pressures. The analysis only has a small discrepancy at the base of the shock. The airfoil upper surface matches all the targets; the lower surface has only a small discrepancy in the cusp region. This case demonstrates that the design method is capable of substantially reproducing a target shape and pressure distribution.

Supercritical Wing With Aeroelastic Effects

After obtaining satisfactory results for the two-dimensional cases, this work was extended to three dimensions. The design algorithm was not modified for three-dimensional applications; it was applied in a streamwise, two-dimensional strip fashion. The calculated pressures, of course, reflect a three-dimensional flow field with sweep, root, and tip effects included. The procedure was repeated for each input wing section, starting with the root section and proceeding out the span.

Figure 10 illustrates the effect of aeroelasticity on a flow over a wing. The results shown are for a station near the tip of the ARW-2 wing. One pressure distribution was computed with aeroelastic effects considered; the other was computed using a rigid wing. For aft-swept configurations, static aeroelastic deflections typically result in negative twist angles, which decrease the lift obtained.

In the following discussion, results from several test cases are shown. These illustrate two methods of accounting for aeroelastic effects, and the problems of designing with no aeroelastic treatment. The first test case involves a design computation in which aeroelastic effects are considered interactively. The second case illustrates a design where aeroelastic effects are not taken into account. The inconsistencies in twist angles result in an unacceptable solution. In the third case, this difficulty is resolved by allowing the sections to rotate during the design process. This leads to an alternate method of accounting for aeroelasticity, the postprocessing method.

For the three-dimensional cases, the ARW-2 wing, a supercritical, aeroelastic wing (Seidel et al., 1985) was used. The ARW-2 is an aft-swept transport-type wing with an aspect ratio of 10.3, a taper ratio of 0.4, and a leading-edge sweep of approximately 27°. A sketch of its planform is shown in figure 11. The 10 streamwise lines across the planform in the figure indicate the stations where the design computations were performed. The fuselage was modeled in the computations as an infinite cylinder.

Target pressures for all cases were generated by analyzing the wing in the WBPPW code at a Mach number of 0.80 and an angle of attack of 1.0° with the TAPS module operating so that aeroelastic effects were included. A structural matrix was generated for the ARW-2 wing using the Engineering Analysis Language (EAL) code (Whetstone, 1983), a finite-element, linear, structural analysis code. For the design work, the supercritical wing sections were replaced with NACA 0006 sections to start the procedure; these sections were twisted to match the ARW-2 geometric twist distribution. The planform was held constant throughout the design process. Three-term smoothing was used. In order to concentrate on aeroelastic effects, viscous effects were not considered in any of these computations.

Case 1—flexible design of ARW-2 wing. The first case includes the TAPS module in the design run so that the aeroelastic deflections are calculated for each design iteration and are reflected in the modifications made to the wing. The results are shown in figures 12 and 13 for 3 of the 10 design stations corresponding to the inboard, planform break, and tip locations. The curve marked "Final" shows the pressures computed during the final design cycle. This curve shows good agreement with the target pressures at all stations. As shown previously, there is some discrepancy at the leading edge due to smoothing. The analysis curve shows pressures computed during an independent analysis of the designed wing. It shows the same agreement with the target pressures as was observed for the final design cycle. This demonstrates that the wing shape produced does achieve the performance predicted by the design procedure.

Figure 13 shows the designed airfoil sections. All the airfoils were slightly thinner than the original sections used to generate the pressures, particularly the tip station. This is possibly a result of starting with the NACA 0006 airfoil, which has a thinner trailing-edge thickness than the ARW-2 sections. Because the first and last points on each surface are fixed and the designed surfaces must be sheared back to conform to these points, the resulting airfoil is thinner than the original. Despite this difference, the surface slopes are closely matched. Even in the cusp region the contours are quite similar for the designs and the original sections. The analysis pressures seen in the previous figure demonstrate that these thinner airfoils are capable of producing the desired pressure distribution.

Case 2—rigid design of ARW-2 wing. The second case shows the results of simply designing to a pressure distribution when that distribution contains aeroelastic effects and there is no procedure in the design method to account for these effects. Figures 14 and 15 show the results at the same stations as the previous case. For the most part, the pressures match the target values closely, especially inboard, where less twisting would be expected to occur. However, at the tip there is a significant difference between target and design in the leading-edge region on the lower surface. The airfoils (fig. 15) follow the same pattern, matching closely inboard but at the tip showing a discrepancy. Since this is

essentially an angle-of-attack problem, matching the target pressures requires moving the stagnation point for the flow forward on the lower surface. This means decreasing the velocity and curvature at the lower surface leading edge and increasing the velocities and curvatures behind it. This results in the bulge seen on the lower surface.

This design case demonstrates the necessity of a procedure for automatically changing the angle of attack of a section (twist). This led to the development of the automatic twisting procedure described previously; the results of its application are shown in the following case.

Case 3—rigid design of ARW-2 wing with automatic twisting. The problem of case 2 was repeated for case 3. The same targets were used, and again no static aeroelastic deflections were calculated within the design computations (TAPS off). The same starting wing shape was used, but this time the automatic twist procedure described previously was employed.

Figures 16 and 17 show the results of this run. The results in figure 16 are essentially the same as those for case 1, with the target pressures again closely matched except for the same small difference at the leading edge. The airfoils also show similar agreement after they are rotated to bring them in line with the target airfoils. The required rotation angles correspond to the deflection angles computed by TAPS in case 1. The differences between the rotation angles computed by the twist procedure and the deflection angles computed by TAPS were 0.19° at the inboard station, 0.02° at the planform break station, and 0.20° at the tip. These results indicate that aeroelasticity need not be iteratively computed inside the design process. Twisting the wing during the design computations would be just as effective. This gives the user two modes for integrating aeroelastic twist into the design.

One option is to use TAPS in the interactive mode to determine aeroelastic twist angles during the design. This method is probably the most straightforward, but it requires prior knowledge of the wing shape and structure for determining a flexibility matrix. This method would be most practical for modifications to existing designs.

The second option is to allow the sections to rotate as needed to reach the desired target pressures. This method would yield a shape and a twist distribution for the wing. The TAPS module could then be used in the postprocessing mode to compute the aeroelastic twist. The total rotation of each section would then be divided into aeroelastic and geometric components. This technique would be the most versatile method and would be easiest to use on a completely new design.

Application of Techniques

The final test case is an application of the method to the task of designing an original wing from a set of arbitrarily defined target pressure distributions. The target pressures were developed to conform to certain design criteria, in contrast to previous cases where they were the result of an analysis of a known shape. Here, aeroelastic effects were taken into account using the postprocessing method described earlier. Viscous effects were determined interactively.

In the initial step toward developing target pressure distributions for this case, a wing was fashioned using a natural laminar flow airfoil section at several stations along a slightly swept and tapered transport-type planform shape (fig. 18). The wing was mounted on an infinite cylinder fuselage. This configuration was then analyzed. The resulting pressure distributions were modified to conform to the design criteria. These criteria included (1) maintaining a favorable pressure gradient over 60 percent of each airfoil, (2) maintaining a local Mach number below 1.2 to delay boundary-layer separation and reduce wave drag, and (3) attempting to obtain an elliptical span loading to reduce induced drag. In order to establish flow parameters, this design was assumed to be for a 10 000-lb aircraft flying at 40 000 ft at a Mach number of 0.78. This yielded a Reynolds number of 8.35 million, a dynamic pressure of 170 lb/ft^2, and a design lift coefficient of 0.45.

Once the target pressures were developed, they were used in a design computation. Again an NACA 0006 airfoil was used as the starting section. This section was combined with the previously described planform and body shape to yield a starting configuration. The automatic twist procedure was in use during this study. The wing design was begun with an angle of attack of 6.1° in order to obtain the necessary lift, but the twist angle of each individual section changed during the design process.

Several iterations of target pressure modification and design work were required to obtain a satisfactory design shape. Target pressures had to be modified to delay separation and to improve designs that were thicker outboard than inboard and airfoil sections that were too thin or even had negative thickness near the trailing edge.

Once a preliminary design was obtained, a flexibility matrix was computed for the wing, using the EAL method described earlier. For ease of computation, the wing was assumed to be solid, but built of a material flexible enough to give a realistic tip deflection. Then further design work was

initiated, this time using the flexibility matrix computed for the intermediate design to allow interactive aeroelastic calculations. Once the design was finalized, a new flexibility matrix was computed and an aeroelastic analysis of the design was performed. Even though the design and analysis used different flexibility matrices, the twist angles computed by TAPS were nearly identical. The changes to the design after the first flexibility matrix was computed were small and did not greatly affect the bending characteristics of the wing or the pressure differentials across the airfoil sections.

Figure 19 shows the pressure distributions obtained in this design exercise. The targets are shown, along with the pressures from the final design cycle and the aeroelastic analysis of the final design shape. Figure 20 shows the final airfoil sections obtained. These results are shown at three stations along the wing: inboard, near the midspan, and near the tip (see fig. 18).

The final and analysis plots show good agreement with the target pressures, matching the shock locations and the pressure levels over most of the design at each location. Only some small discrepancies in the aft part of the distributions are noted. Designing realistic pressure distributions in this area was found to be a very difficult task. The designer must allow adequate airfoil thickness without causing separation. For the midspan section and the section near the tip, the upper surface leading-edge design and analysis pressures show a discrepancy with the targets. This is due to smoothing. The results shown were obtained using three-term smoothing. Rerunning the case with five-term smoothing gave a much better match for the tip station, but for the section near the root gave a discrepancy in the leading-edge region of the lower surface.

The span load distribution is shown in figure 21. The distribution obtained is not far from the design goal of elliptic. The analysis run results estimate the efficiency factor at 0.998.

Some timing studies were done with this case. The work was done on a Cray Y-MP computer. The targets, analyses, and designs were run for 200 crude and 1000 crude/fine iterations. All runs included interactive boundary-layer calculations. For the initial design cases, where TAPS was not employed, 877 cpu seconds were required. When TAPS was included, in the later designs, 895 cpu seconds were used. The TAPS-on analyses used 721 cpu seconds.

Figures 19 and 20 might be considered part of a series of working plots that a designer would use to obtain an acceptable wing design. While many important aerodynamic criteria were adhered to in developing this design, there may be other considerations that should be taken into account to incorporate this into the total aircraft design. Balancing these considerations generally requires a number of iterations of modifications to the target pressures followed by design runs, so that developing an appropriate set of target pressure distributions becomes the goal of the designer.

Concluding Remarks

The effects of viscosity and aeroelastic deflections on wings at transonic speeds can be significant. A transonic design method has been developed for two-dimensional airfoils and three-dimensional wings; it includes techniques that can account for both viscous effects and aeroelastic deflections. Included in this work are suggestions for both interactive and postdesign techniques of accounting for these effects. This procedure is capable of designing either conventional or supercritical sections.

Test cases are shown to demonstrate the viability of the method. Known airfoil sections and wings were analyzed to generate target pressure distributions, which were used as input for the design process. The designs obtained generally matched the target pressures and the airfoils used to generate them. Only small discrepancies are noted, usually near the leading edge where the smoothing procedure distorted the airfoil shape. The shock locations and the cusp regions were accurately reproduced by the method, even when viscous or aeroelastic effects were included. Interactive methods of accounting for viscous and aeroelastic effects were found to be the most accurate and easiest to use but required slightly more cpu time.

Developing realistic target pressures for an arbitrary design was found to be a difficult task. Many factors must be taken into consideration when developing a target pressure distribution to ensure that it will yield a realistic design. The exercise is best approached as an iterative procedure, using the results of design runs to guide modifications to the pressures.

NASA Langley Research Center
Hampton, VA 23665-5225
November 9, 1990

Appendix

Convergence Considerations

During development of the design method, it was noted that it was not unusual for a three-dimensional design case to require 200 crude and 2300 crude/fine grid iterations through the aerodynamic module before a final design was obtained. This was many more iterations than were being used to determine the target pressure distributions. A study was performed to determine how many iterations in the aerodynamic analysis module were required to adequately establish the pressure distribution. In the following discussion, iterations through the code are expressed as "a/b". This reflects a initial crude grid iterations and b iterations using both the crude and fine grids.

A section of the ARW-2 wing was used for this study. It was analyzed in the WBPPW code using increasingly larger numbers of iterations to determine the level at which the pressure distribution ceased to change. First, 100/80 iterations were used, conforming to the recommendations of Boppe (1987). Next, this was increased to 200/300 and 200/1000. Finally, 200/2000 and 200/2400 were used to bracket the number of iterations typically used in a design case.

For comparison purposes, a second wing was generated by using the same planform as the ARW-2, but replacing its supercritical sections with a more conventional section, an NACA 64_a012. This wing was also analyzed using the pattern of iterations listed above. Both three-dimensional cases were run at a Mach number of 0.8. The ARW-2 wing was run at an angle of attack of $-1.0°$ and the convention section wing at 2.0°, to obtain a wing C_L near 0.55 at the intermediate levels of iterations for both cases.

Finally, a similar study was conducted for 2 two-dimensional airfoils, the NACA 64_a012 section, and a supercritical section near the tip of the ARW-2. The two-dimensional cases were run at a Mach number of 0.75 and a value of c_l near 0.55.

The analysis code was found to require a higher number of iterations for convergence than was recommended by Boppe (1987). Figure A1 shows computed pressure distributions for the cases listed above. Figure A1(a) presents the results from the ARW-2 case, and figure A1(b) shows the results obtained when the supercritical sections were replaced with conventional sections. For both cases, pressures near the tip ($\eta = 0.90$) are shown. The figures clearly show that under these conditions the solution is not converged for the first two levels of iterations tested. There are significant differences between the magnitudes of the pressures computed at each of the first three iteration levels. At the level of 200/1000 and above, however, the differences between the levels appear to be small. For this reason, the target pressures for the three-dimensional example cases shown in the paper are computed with 200/1000 iterations.

Figures A1(c) and A1(d) show convergence in the two-dimensional mode. Figure A1(c) shows results from an analysis of a supercritical section of the ARW-2 wing, and figure A1(d) shows a two-dimensional analysis of the NACA 64_a012 airfoil. The results here are even more dramatic. The differences in the solutions do not become small until the last two levels.

The aerodynamic analysis code used in this method was found to require more iterations for convergence than was previously thought. This was taken into account, and target pressures were obtained at levels of convergence corresponding to the design procedure. For actual applications the large number of iterations required for a design will generally ensure that the results are converged enough for engineering accuracy.

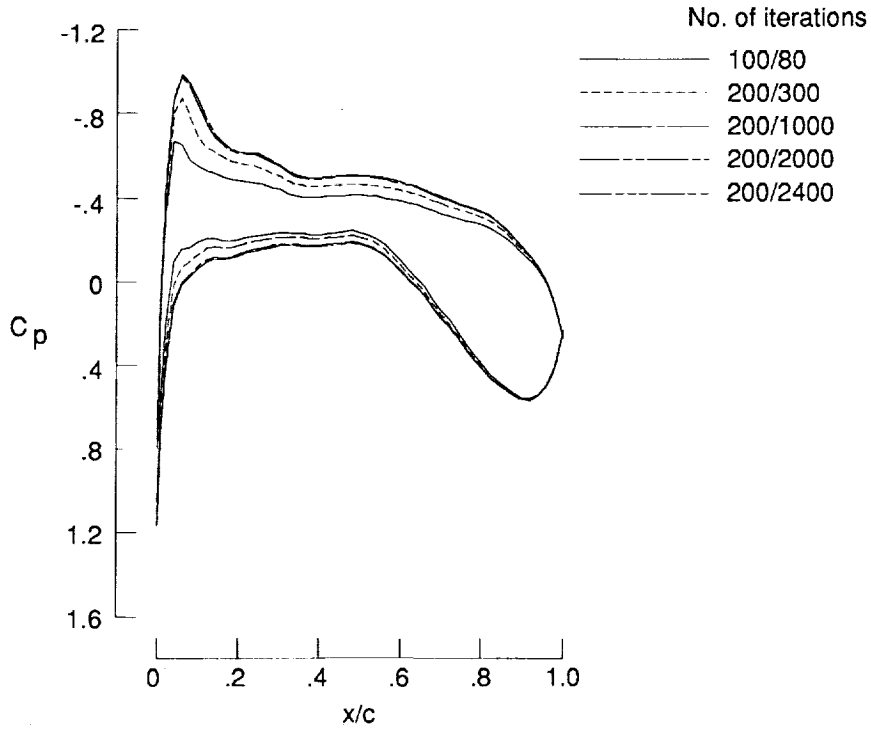

(a) 3-D ARW-2; $M = 0.8$, $\alpha = -1.0°$, $C_L \approx 0.55$.

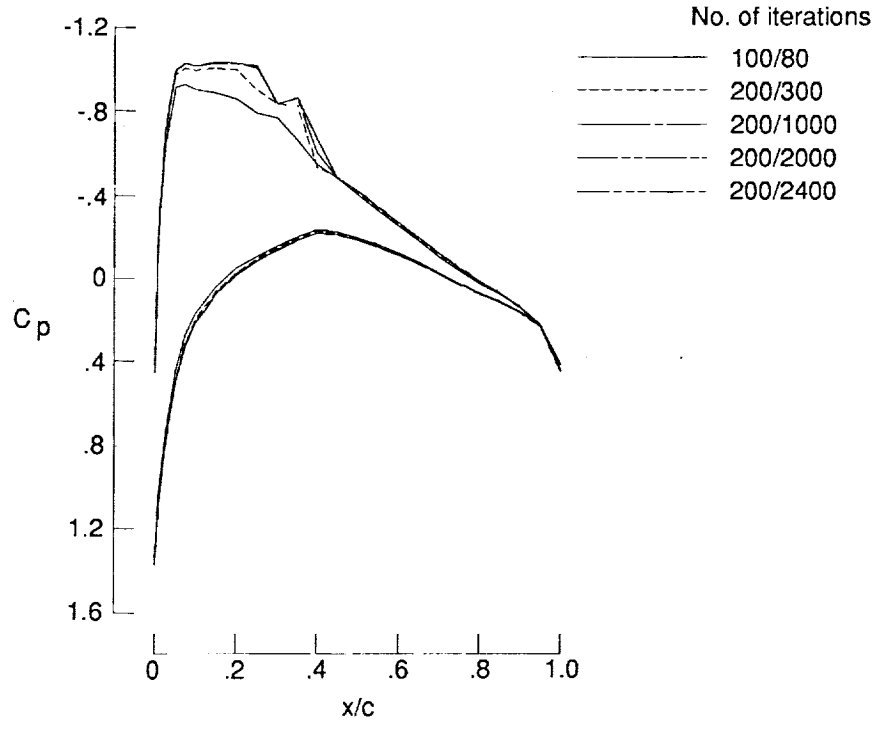

(b) 3-D conventional section; $M = 0.8$, $\alpha = 2.0°$, $C_L \approx 0.55$.

Figure A1. WBPPW convergence history study; $\eta = 0.9$.

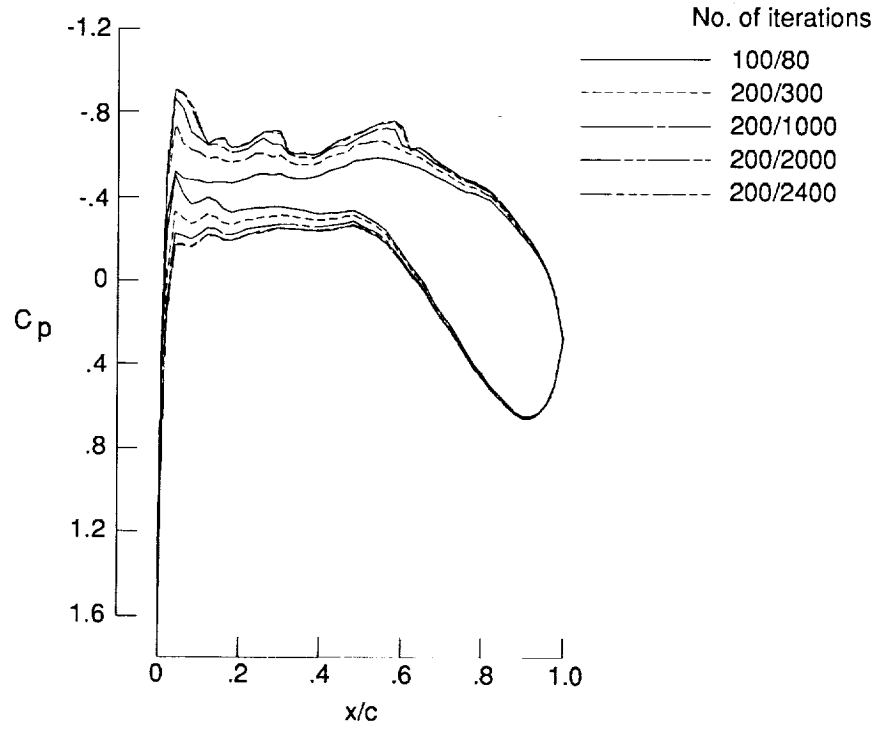

(c) 2-D supercritical section; $M = 0.75$, $\alpha = -1.0°$, $c_l \approx 0.55$.

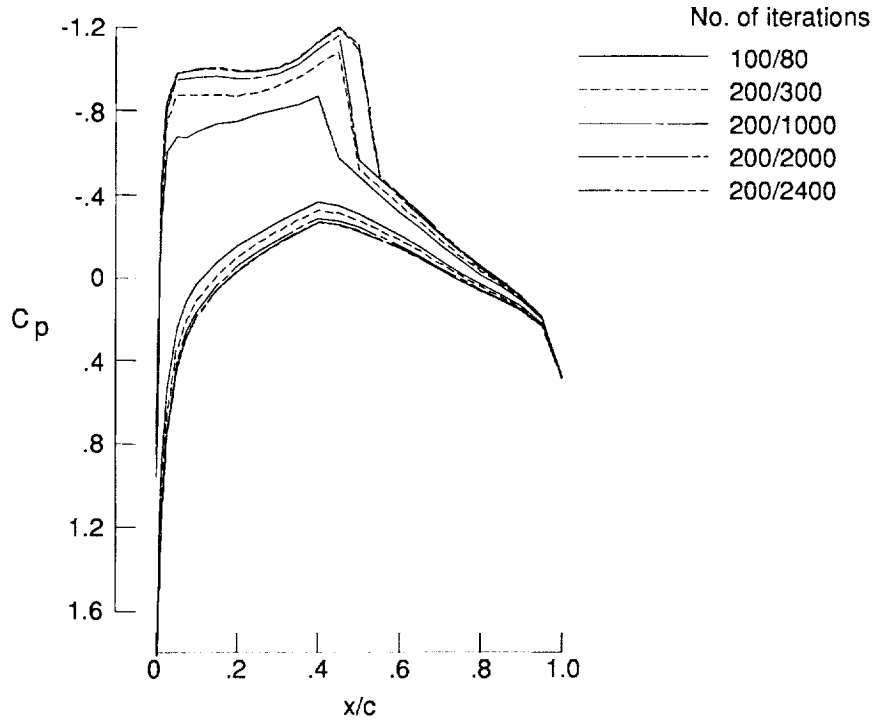

(d) 2-D conventional section; $M = 0.75$, $\alpha = 2.0°$, $c_l \approx 0.55$.

Figure A1. Concluded.

References

Barger, Raymond L.; and Brooks, Cuyler, W., Jr., 1974: *A Streamline Curvature Method for Design of Supercritical and Subcritical Airfoils.* NASA TN D-7770.

Bauer, F.; Garabedian, P.; and Korn, D. 1972: *A Theory of Supercritical Wing Sections, With Computer Programs and Examples.* Volume 66 of *Lecture Notes in Economics and Mathematical Systems,* M. Beckmann and H. P. Künzi, eds., Springer-Verlag.

Boppe, Charles W. 1987: *Aerodynamic Analysis for Aircraft With Nacelles, Pylons, and Winglets at Transonic Speeds.* NASA CR-4066.

Bradshaw, P.; and Ferriss, D. H. 1971: Calculation of Boundary-Layer Development Using the Turbulent Energy Equation: Compressible Flow on Adiabatic Walls. *J. Fluid Mech.*, vol. 46, pt. 1, Mar. 15, pp. 83–110.

Campbell, Richard L. 1984: Calculated Effects of Varying Reynolds Number and Dynamic Pressure on Flexible Wings at Transonic Speeds. Recent Experiences in Multidisciplinary Analysis and Optimization, Jaroslaw Sobieski, compiler, NASA CP-2327, Part 1, pp. 309–327.

Campbell, Richard L.; and Smith, Leigh A. 1987: A Hybrid Algorithm for Transonic Airfoil and Wing Design. AIAA-87-2552-CP, Aug.

Davis, Warren H., Jr., 1979: Technique for Developing Design Tools From the Analysis Methods of Computational Aerodynamics. AIAA Paper 79-1529, July.

Hicks, Raymond M.; Murman, Earll M.; and Vanderplaats, Garret N. 1974: *An Assessment of Airfoil Design by Numerical Optimization.* NASA TM X-3092.

Kennelly, Robert A., Jr. 1983: Improved Method for Transonic Airfoil Design-by-Optimization. AIAA-83-1864, July.

Liepmann, H. W.; and Roshko, A. 1957: *Elements of Gasdynamics.* John Wiley & Sons, Inc.

Seidel, David A.; Sandford, Maynard C.; and Eckstrom, Clinton V. 1985: *Measured Unsteady Transonic Aerodynamic Characteristics of an Elastic Supercritical Wing With an Oscillating Control Surface.* NASA TM-86376.

Sobieczky, H.; Yu, N. J.; Fung, K.-Y.; and Seebass, A. R. 1979: New Method for Designing Shock-Free Transonic Configurations. *AIAA J.,* vol. 17, no. 7, July, pp. 722–729.

Tranen, T. L. 1974: A Rapid Computer Aided Transonic Airfoil Design Method. AIAA Paper No. 74-501, June.

Vanderplaats, Garret N. 1973: *CONMIN—A FORTRAN Program for Constrained Function Minimization, User's Manual.* NASA TM X-62282.

Volpe, G.; and Melnik, R. E. 1985: A Method for Designing Closed Airfoils for Arbitrary Supercritical Speed Distributions. AIAA-85-5023, Oct.

Whetstone, W. D. 1983: *EISI-EAL Engineering Analysis Language Reference Manual—EISI-EAL System Level 2091. Volume 1: General Rules and Utility Processors.* Engineering Information Systems, Inc., July.

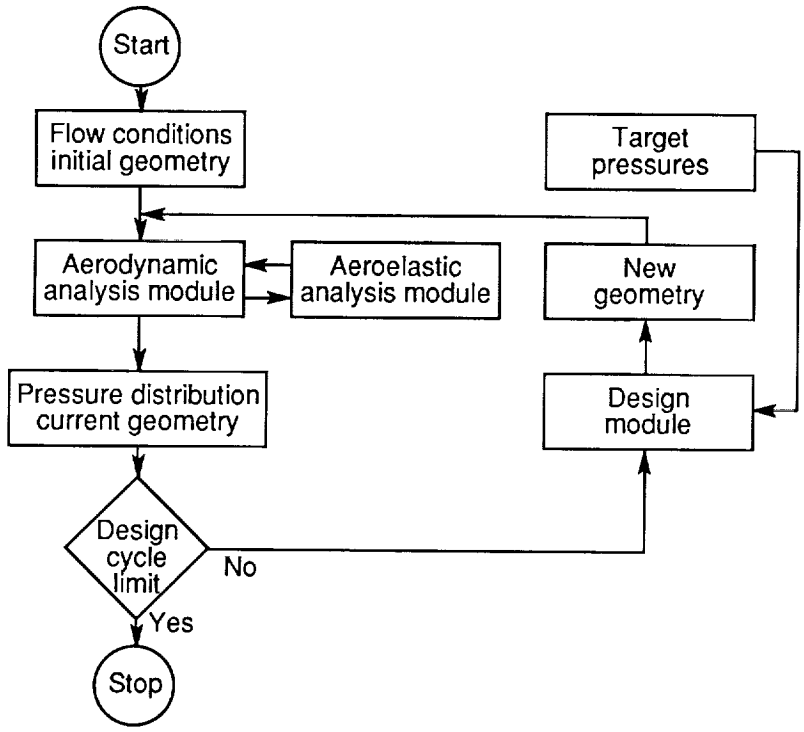

(a) With interactive mode.

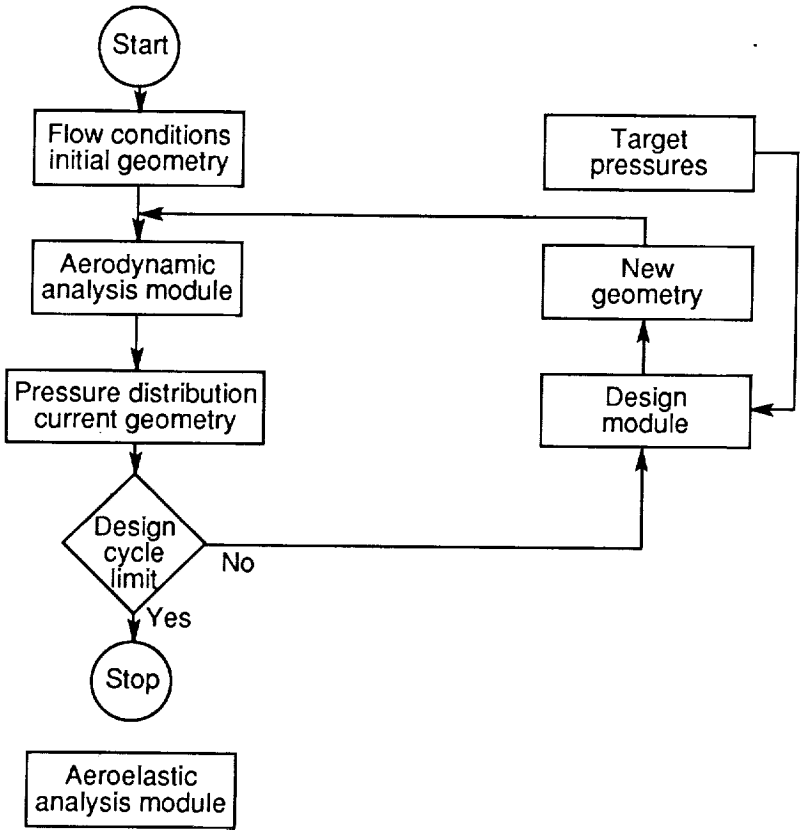

(b) With postprocessing mode.

Figure 1. Automated predictor/corrector design method with aeroelastic effects.

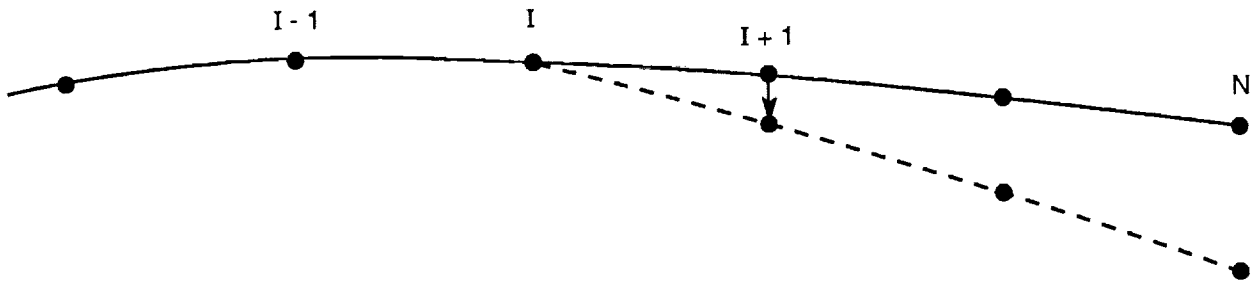

(a) Method of changing curvature at one point only.

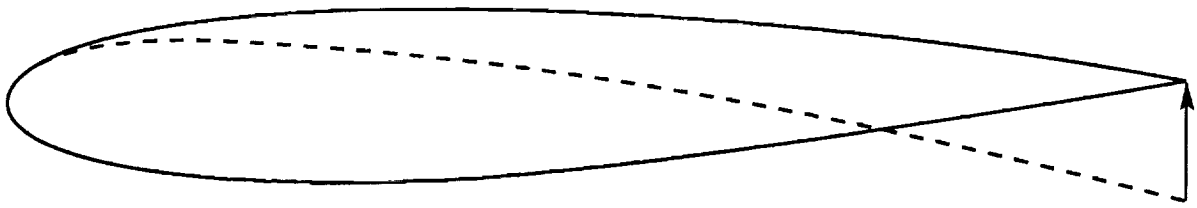

(b) Shear about leading edge to maintain trailing-edge thickness.

Figure 2. Airfoil geometry modification procedure.

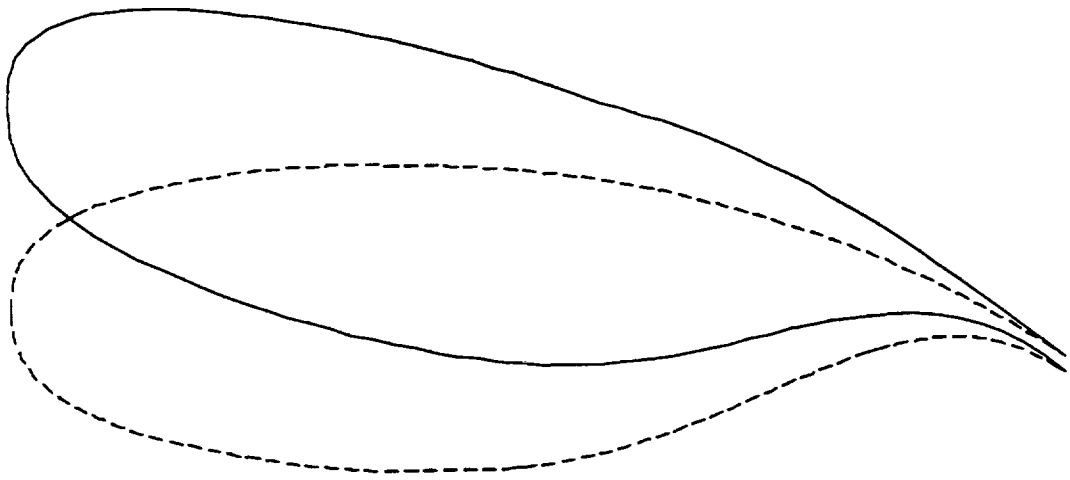

(a) Global effects.

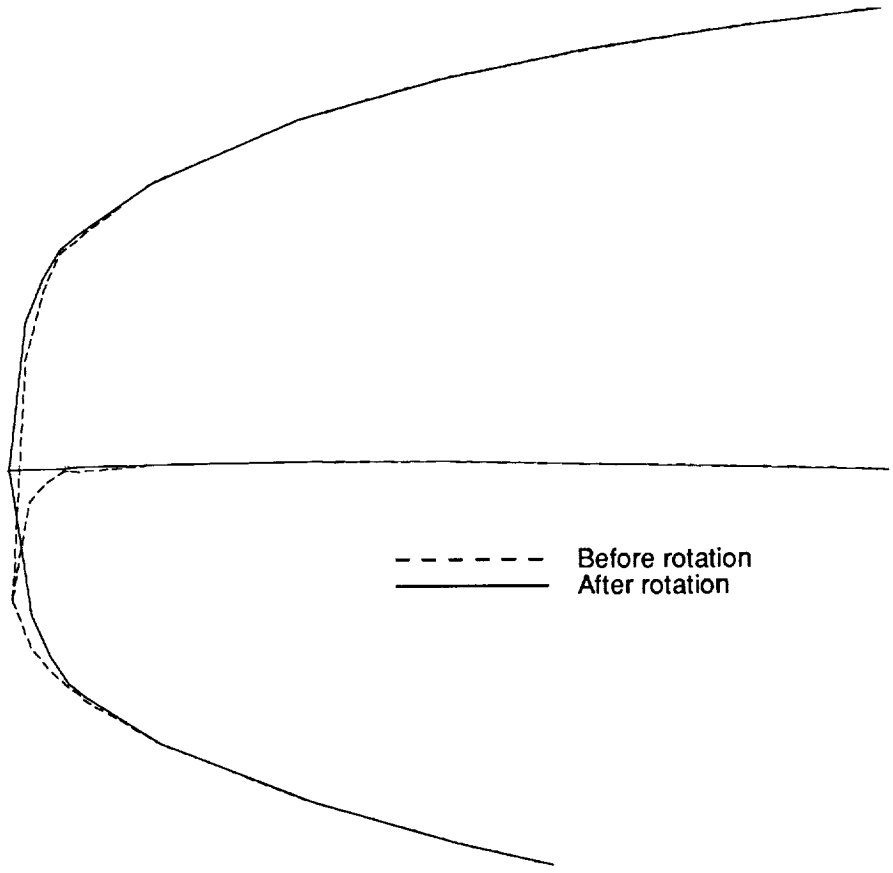

(b) Nose region.

Figure 3. Effects of smoothing on airfoil orientation.

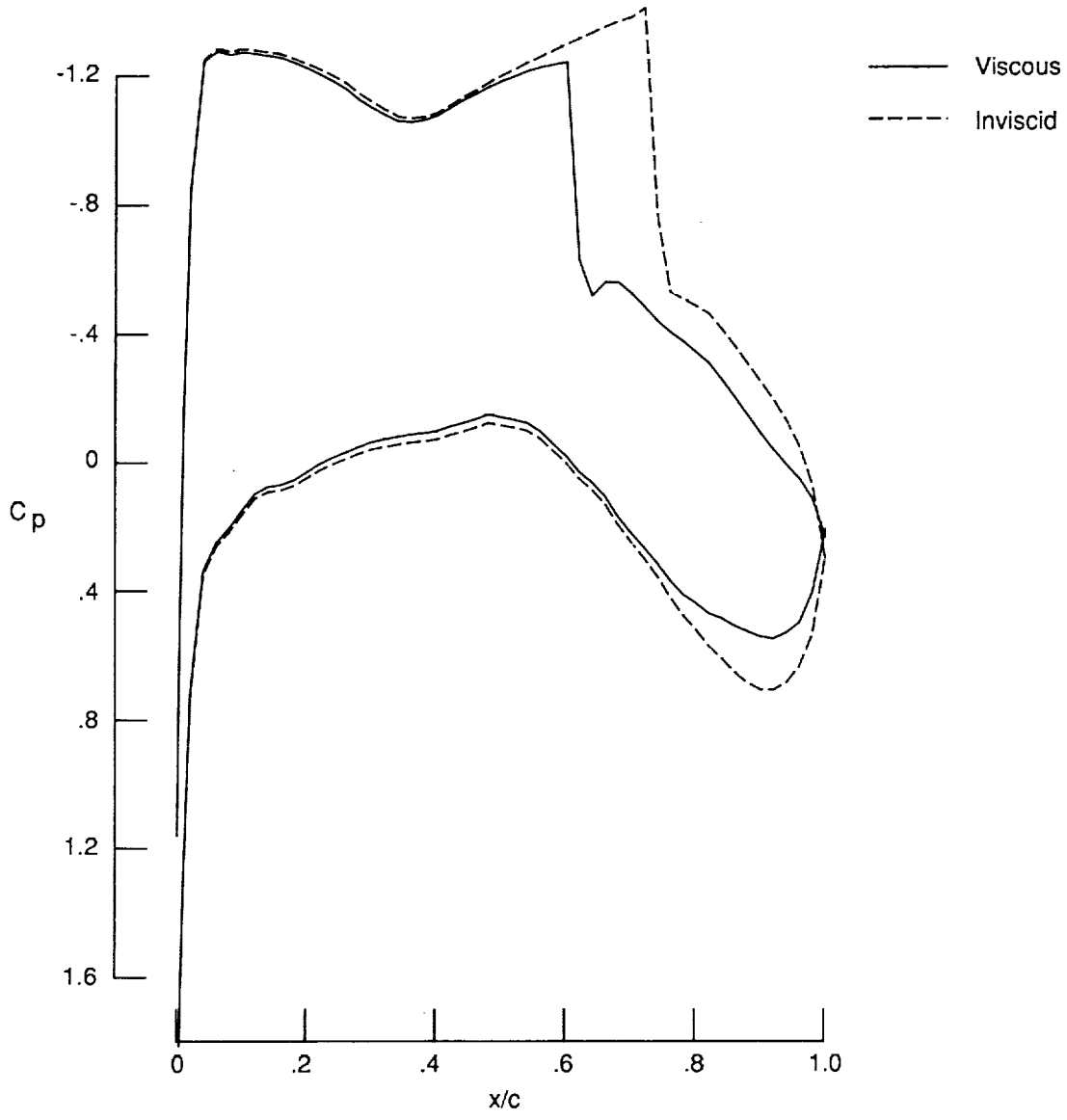

Figure 4. Effect of viscosity on a supercritical airfoil; $M = 0.77$, $\alpha = 1.0$, $R = 5.0 \times 10^6$.

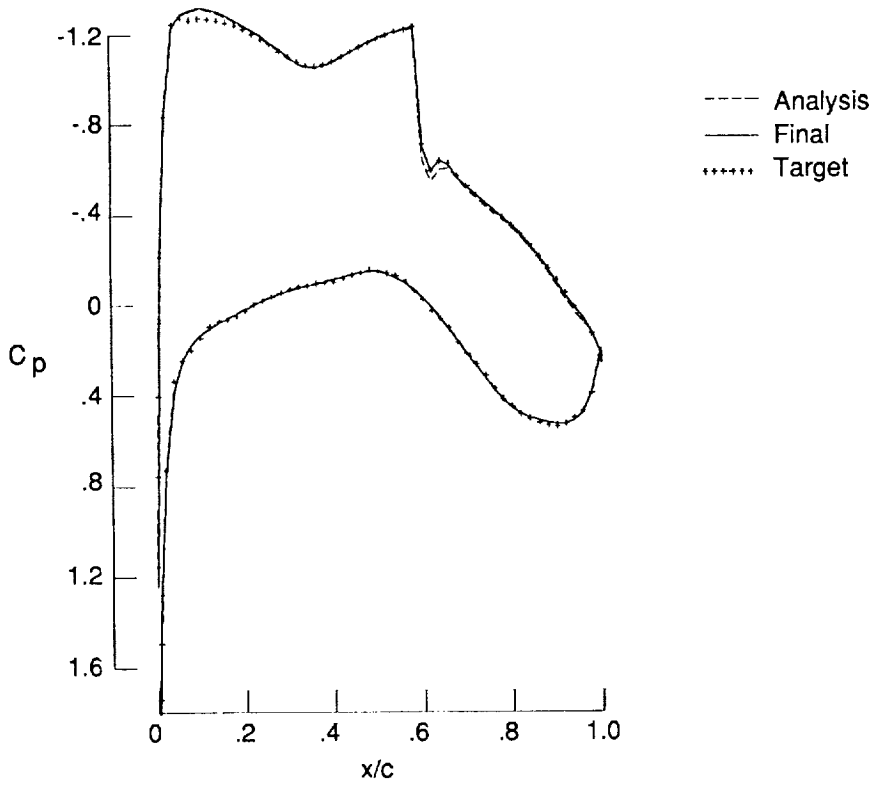

(a) Pressure distribution.

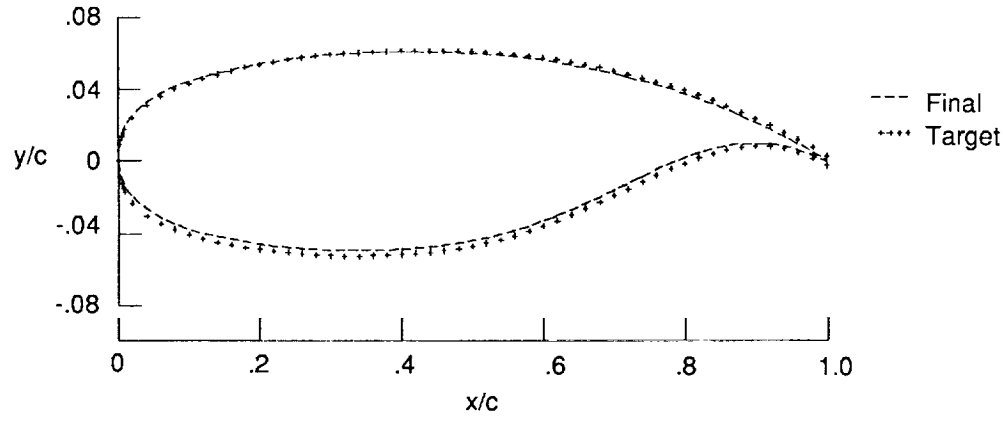

(b) Airfoil coordinates.

Figure 5. Supercritical airfoil design case with interactive viscous effects; $M = .077$, $\alpha = 1.0$, $R = 5.0 \times 10^6$.

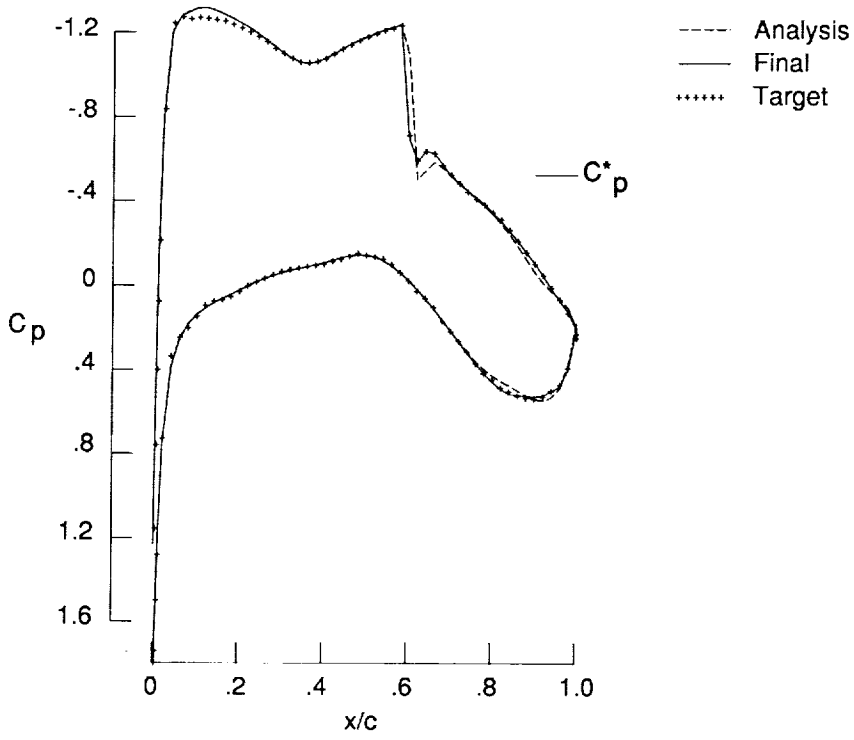

(a) Pressure distribution.

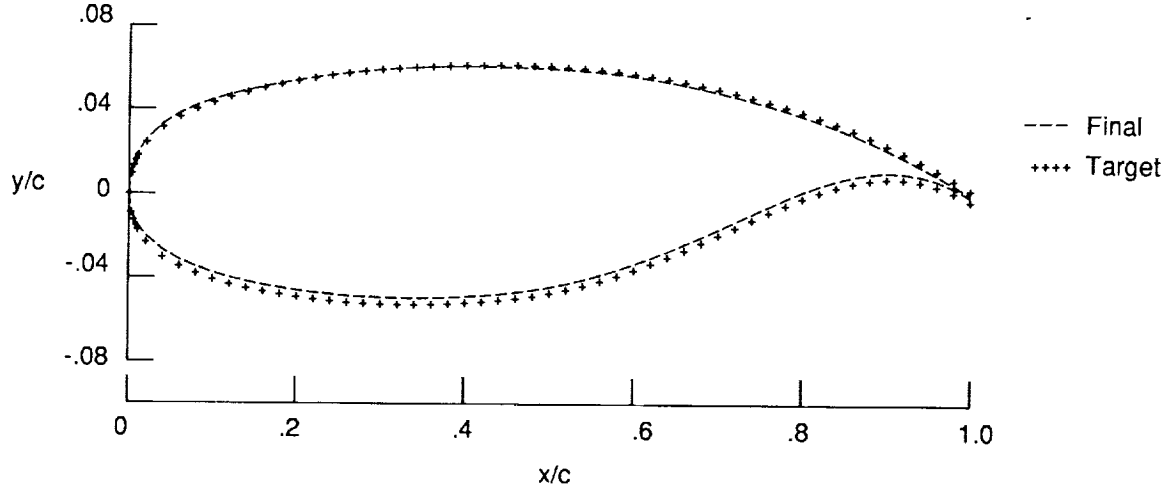

(b) Airfoil coordinates.

Figure 6. Supercritical airfoil design case with postprocessing of viscous effects; $M = 0.77$, $\alpha = 1.0$, $R = 5.0 \times 10^6$.

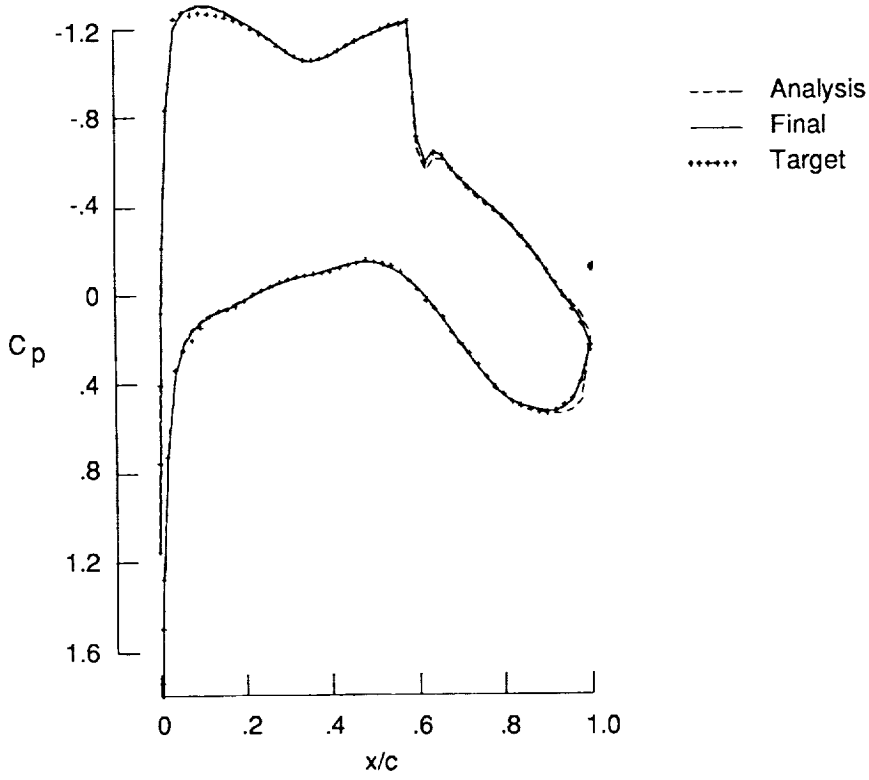

(a) Pressure distribution.

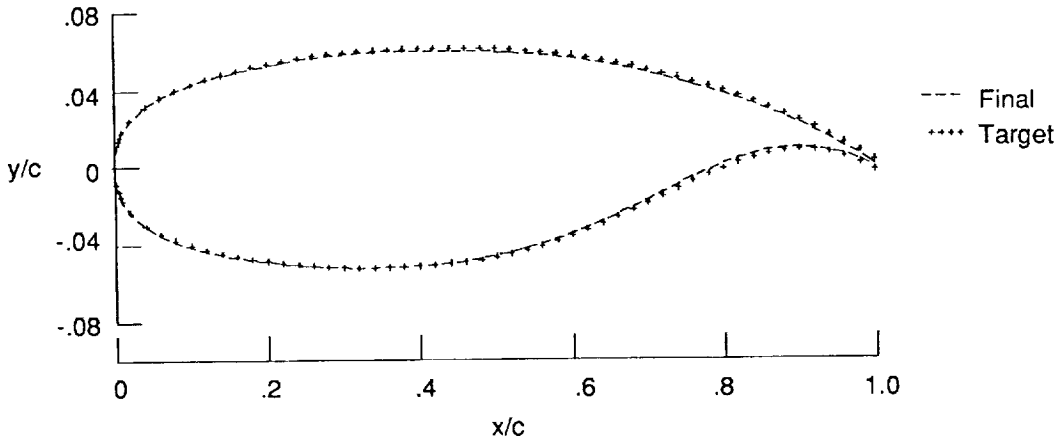

(b) Airfoil coordinates.

Figure 7. Supercritical design case with interactive viscous effects and automatic twisting; $M = 0.77$, $\alpha = 1.0$, $R = 5.0 \times 10^6$.

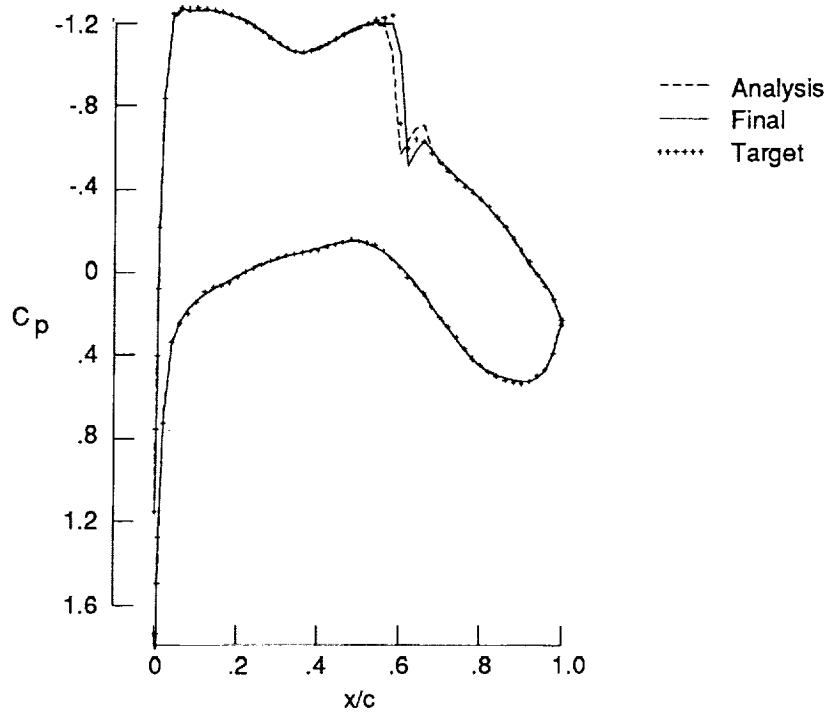

(a) Pressure distribution.

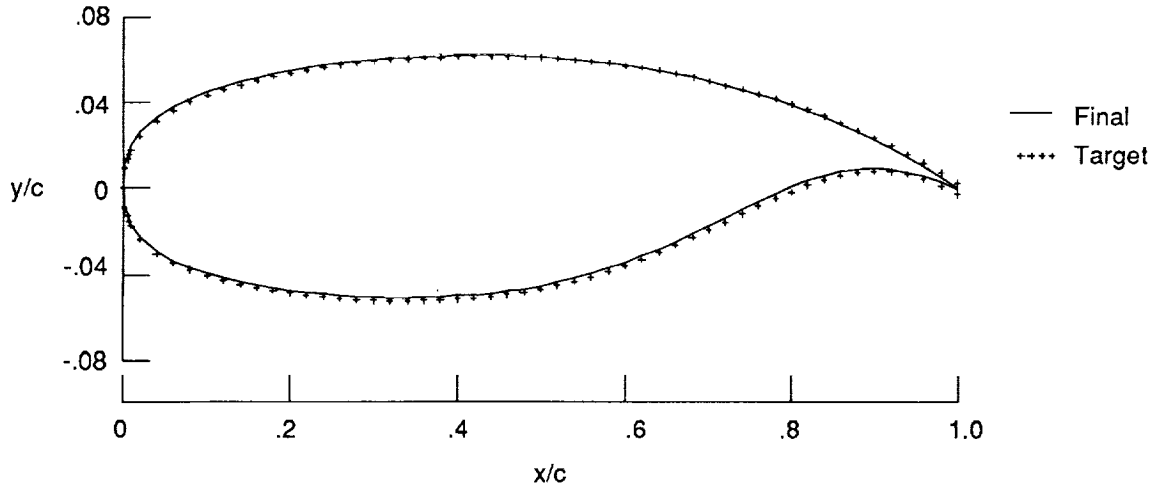

(b) Airfoil coordinates.

Figure 8. Supercritical design case with interactive viscous effects, automatic twisting, and five-term smoothing; $M = 0.77$, $\alpha = 1.0$, $R = 5.0 \times 10^6$.

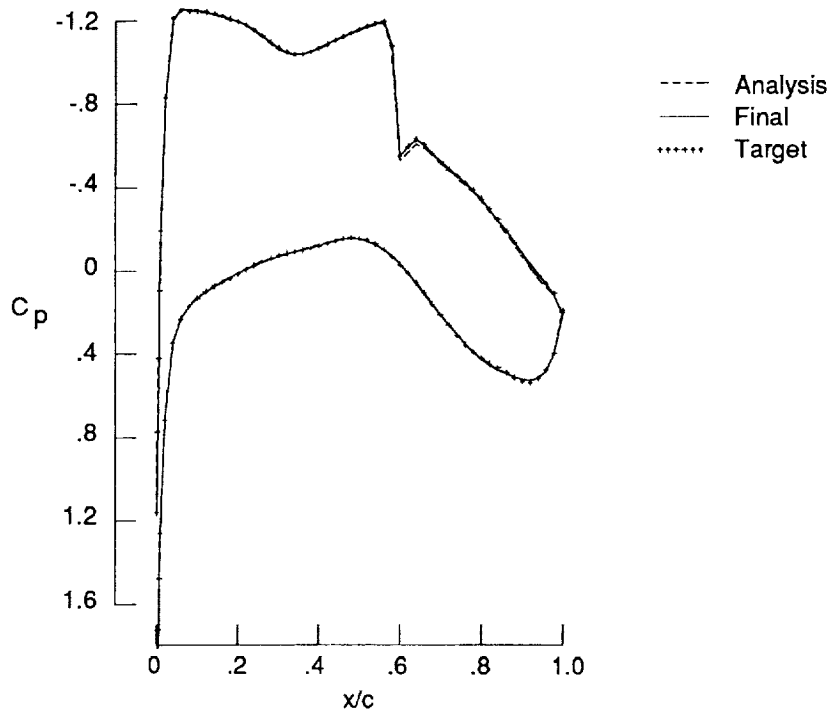

(a) Pressure distribution.

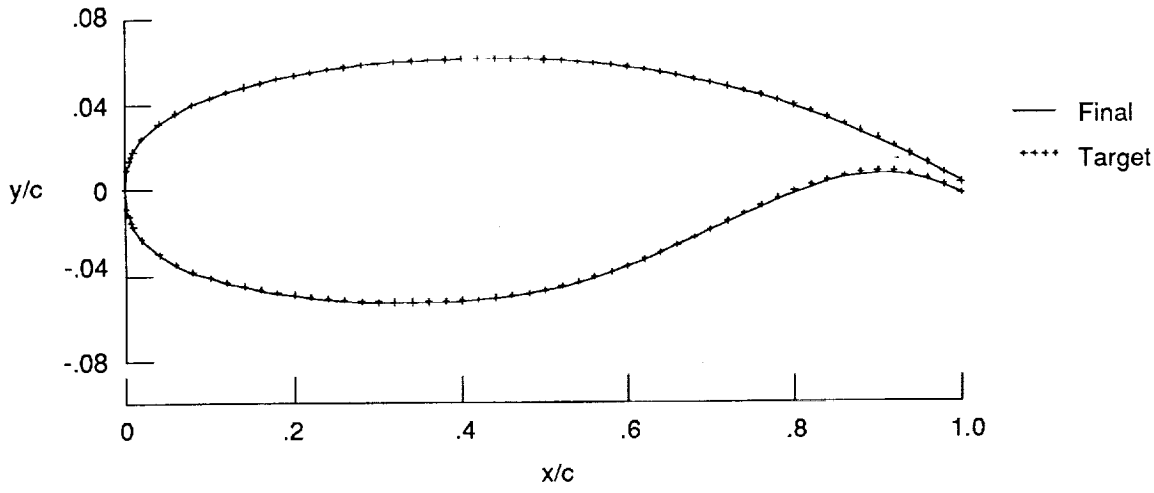

(b) Airfoil coordinates.

Figure 9. Supercritical design case for presmoothed airfoil; $M = 0.77$; $\alpha = 1.0$, $R = 5.0 \times 10^6$.

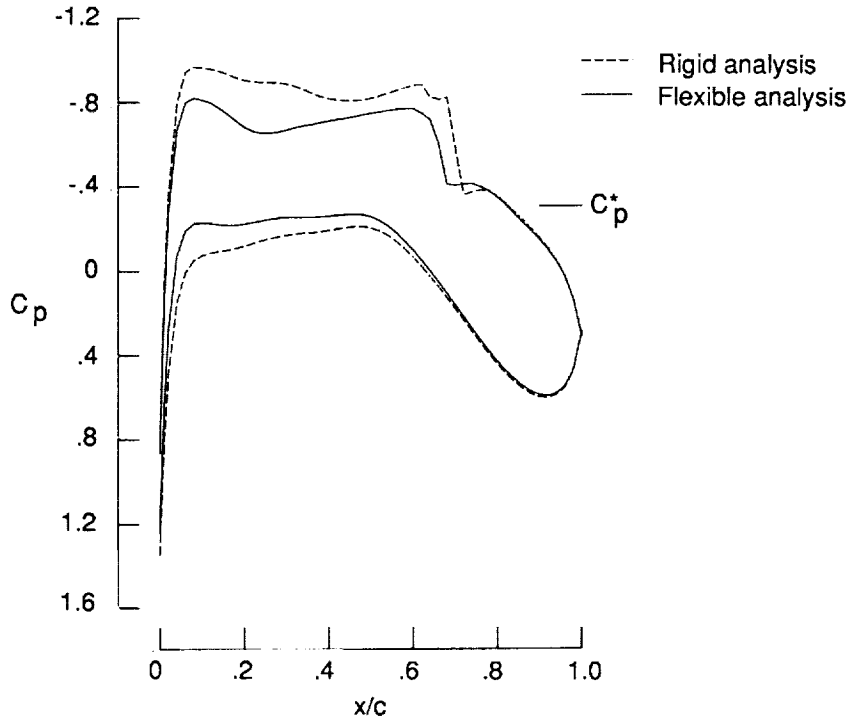

Figure 10. Effect of aeroelasticity on a section of a supercritical wing; $M = 0.80$; $\alpha = 1.0$.

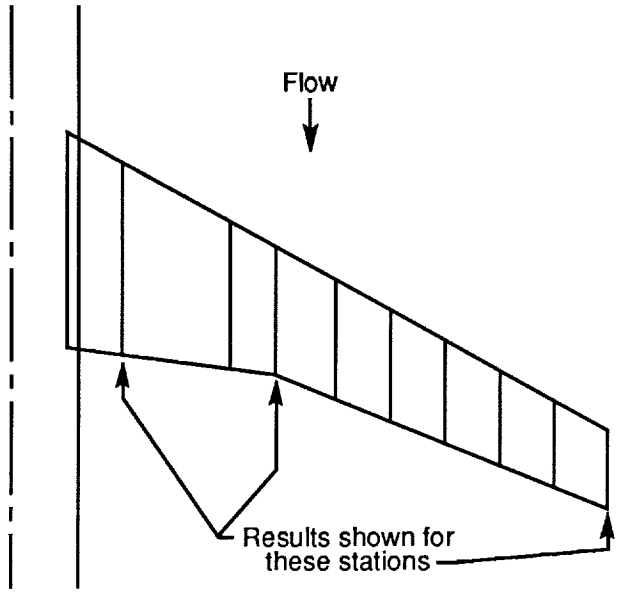

Figure 11. ARW-2 wing geometry.

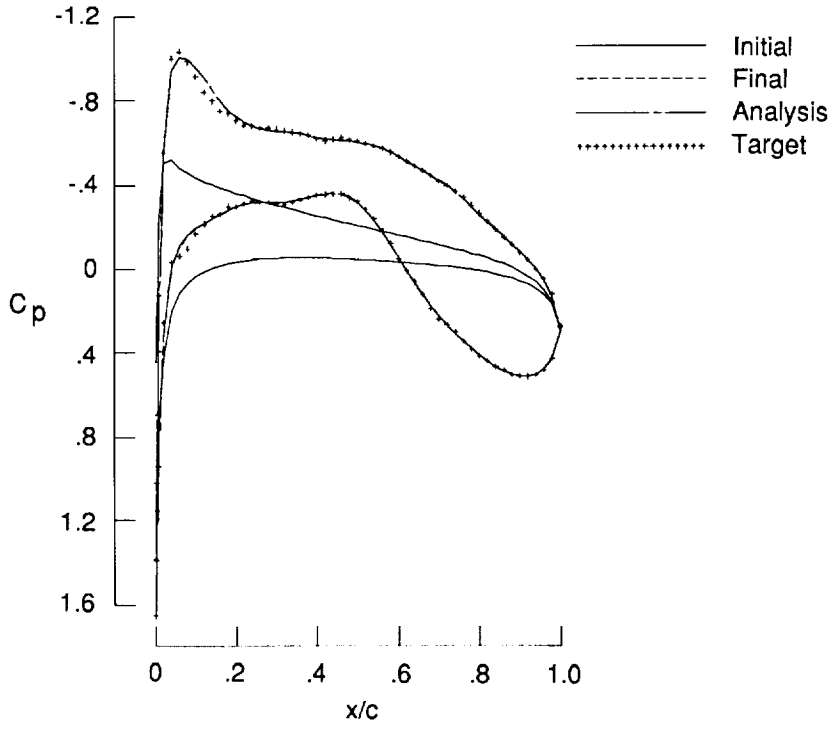

(a) Inboard; $\eta = 0.18$.

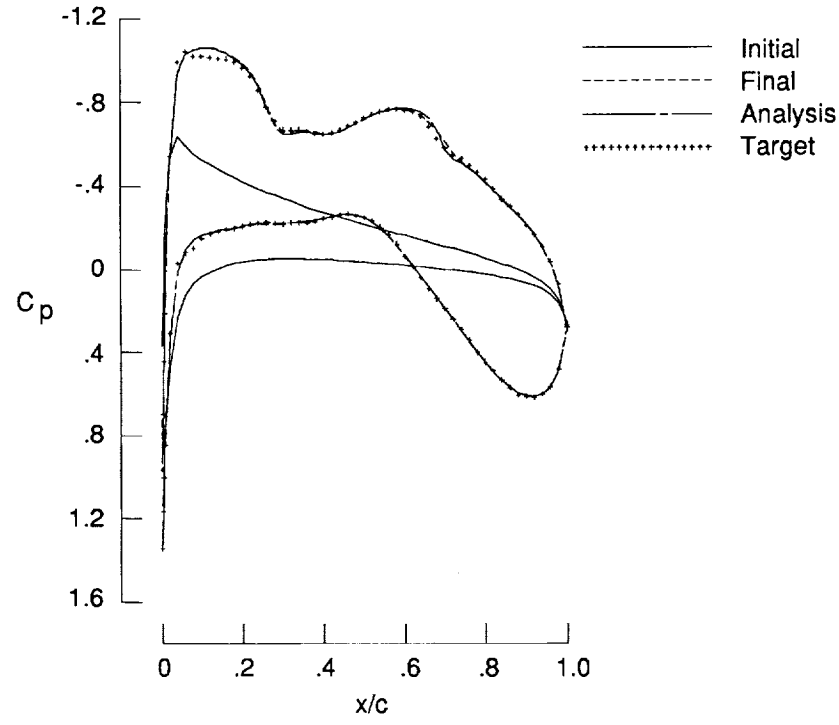

(b) Planform break; $\eta = 0.44$.

Figure 12. Pressure distributions for the aeroelastic design case; $M = 0.80$, $\alpha = 1.0$.

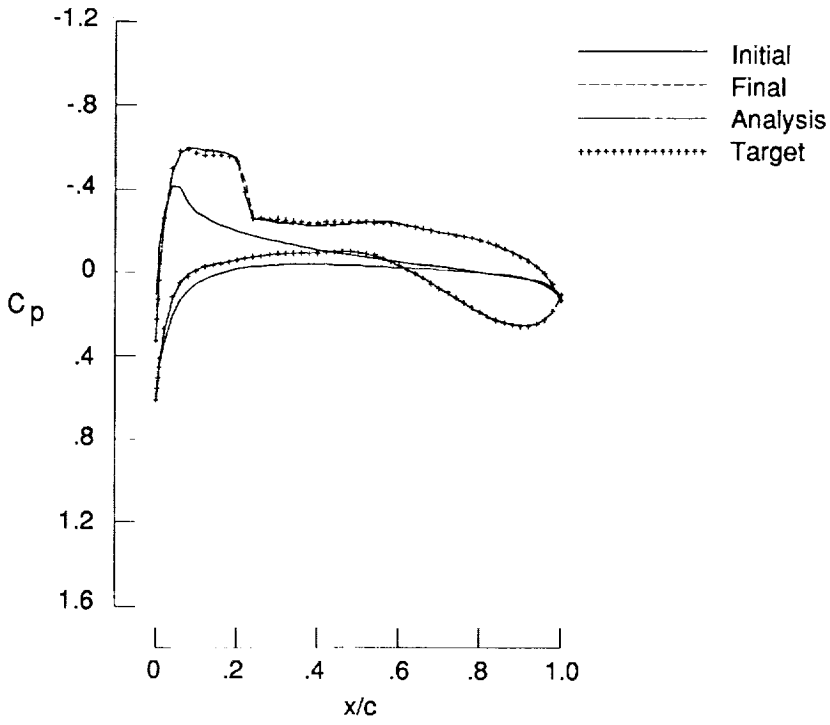

(c) Wingtip; $\eta = 1.0$.

Figure 12. Concluded.

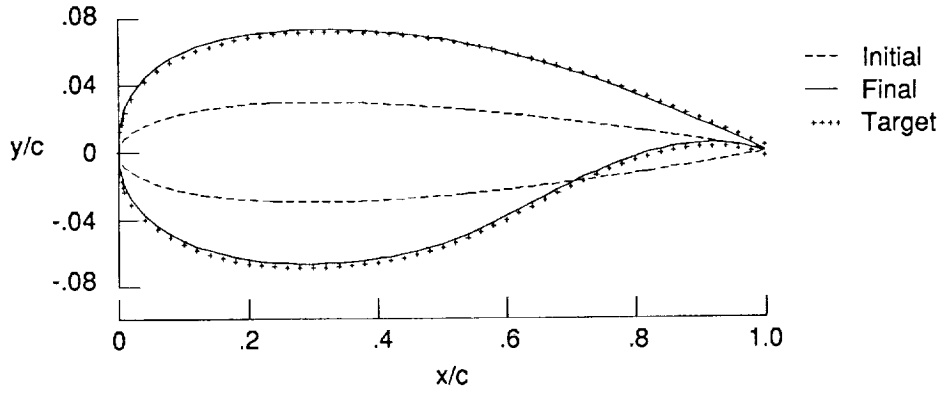

(a) Inboard; $\eta = 0.18$.

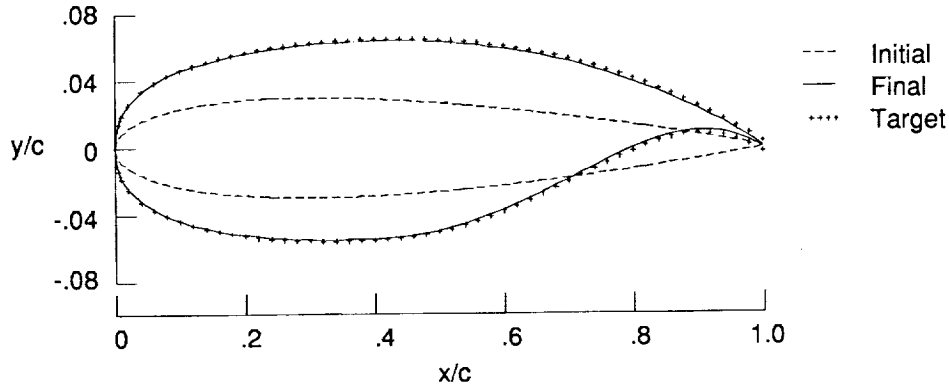

(b) Planform break; $\eta = 0.44$.

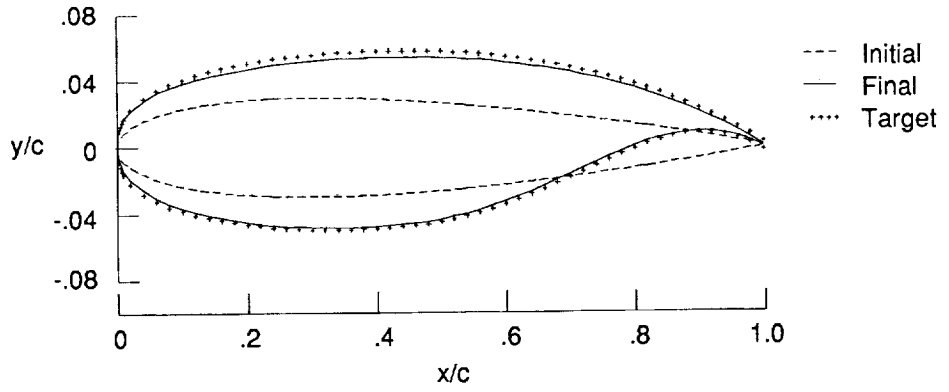

(c) Wingtip; $\eta = 1.0$.

Figure 13. Airfoil coordinates for the aeroelastic design case; $M = 0.80$, $\alpha = 1.0$.

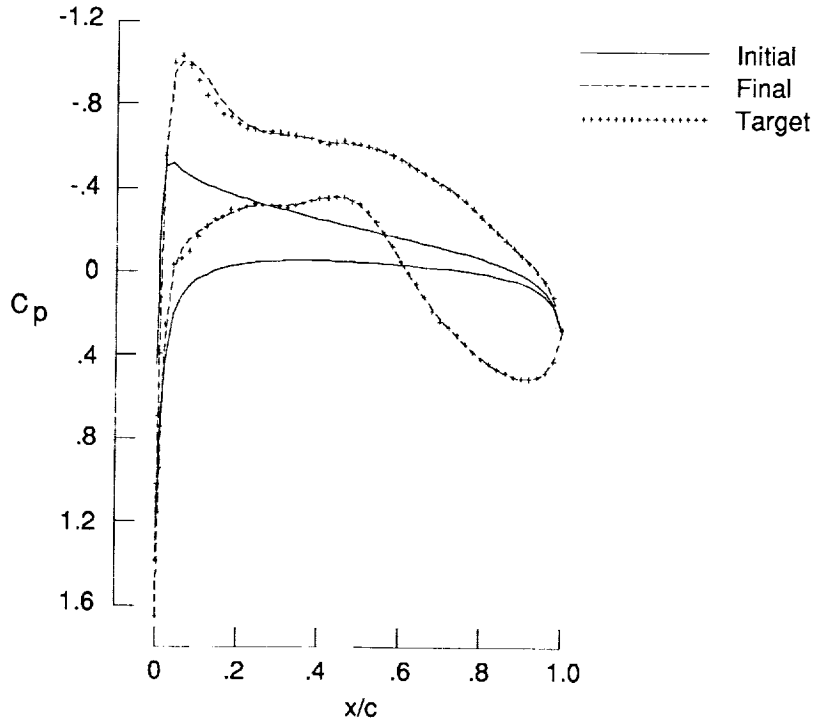

(a) Inboard; $\eta = 0.18$.

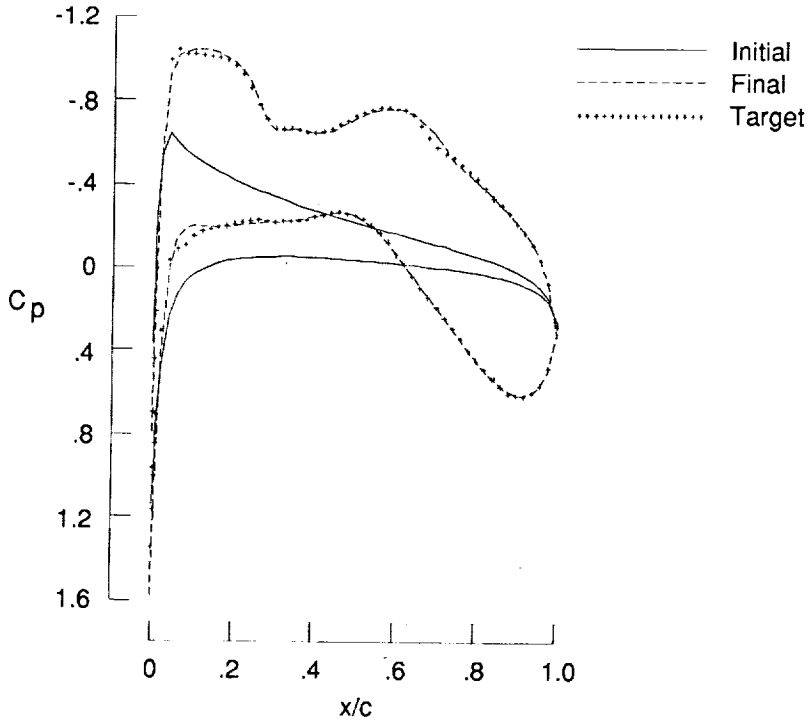

(b) Planform break; $\eta = 0.44$.

Figure 14. Pressure distributions for the rigid design case; $M = 0.80$, $\alpha = 1.0$.

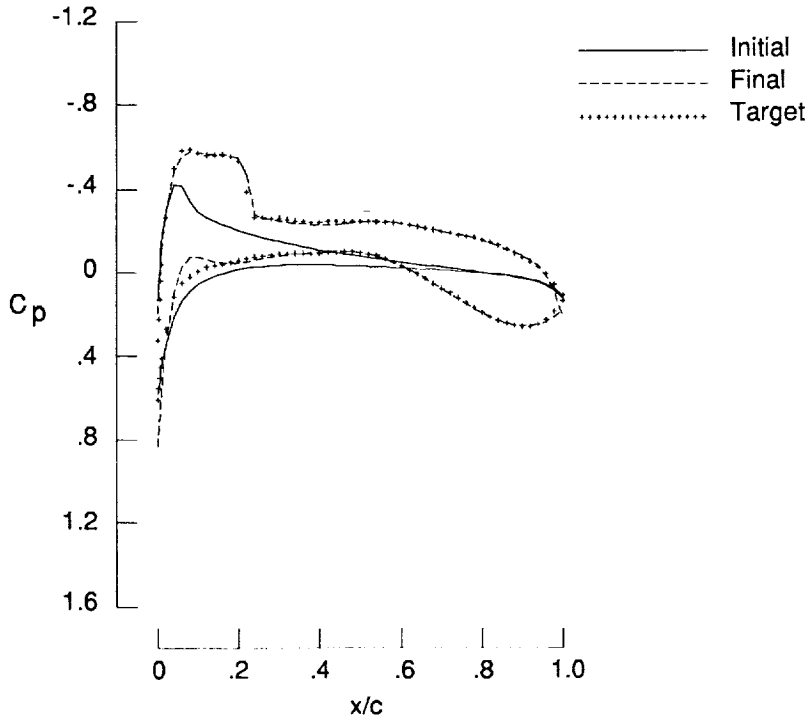

(c) Wingtip; $\eta = 1.0$.

Figure 14. Concluded.

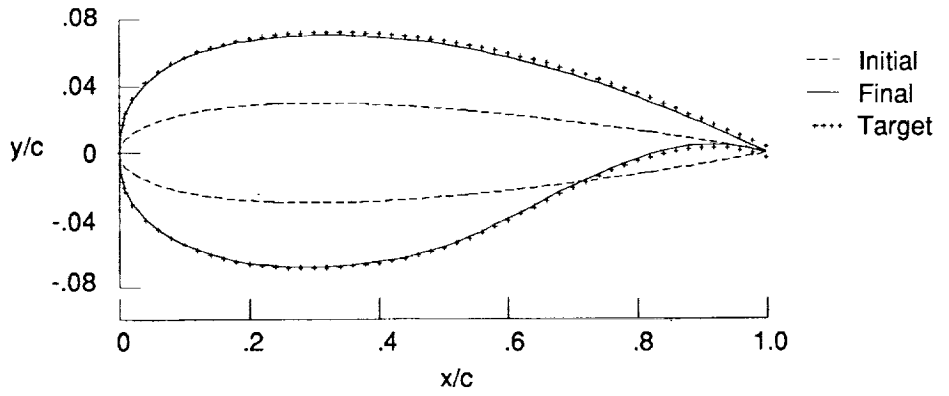

(a) Inboard; $\eta = 0.18$.

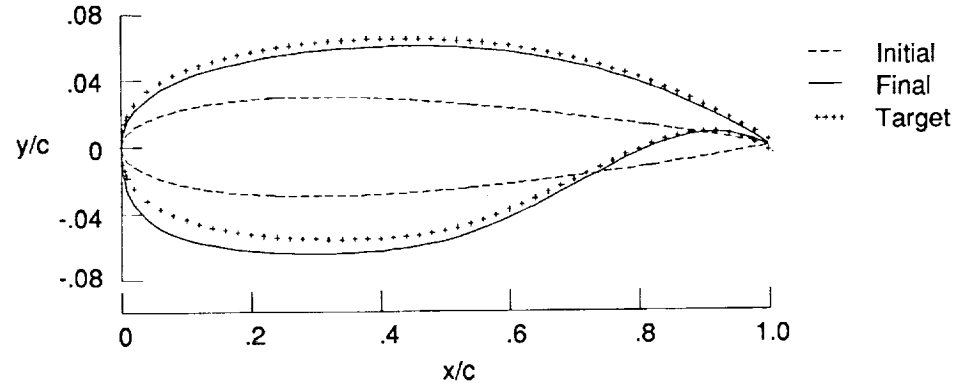

(b) Planform break; $\eta = 0.44$.

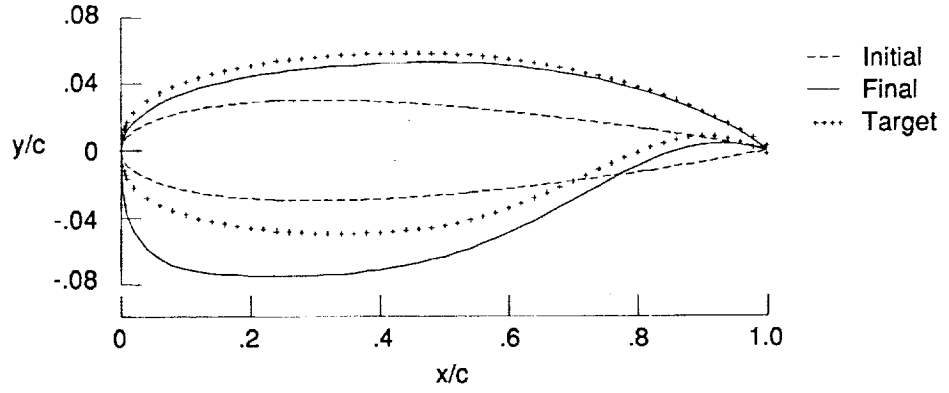

(c) Wingtip; $\eta = 1.0$.

Figure 15. Airfoil coordinates for the rigid design case; $M = 0.80$, $\alpha = 1.0$.

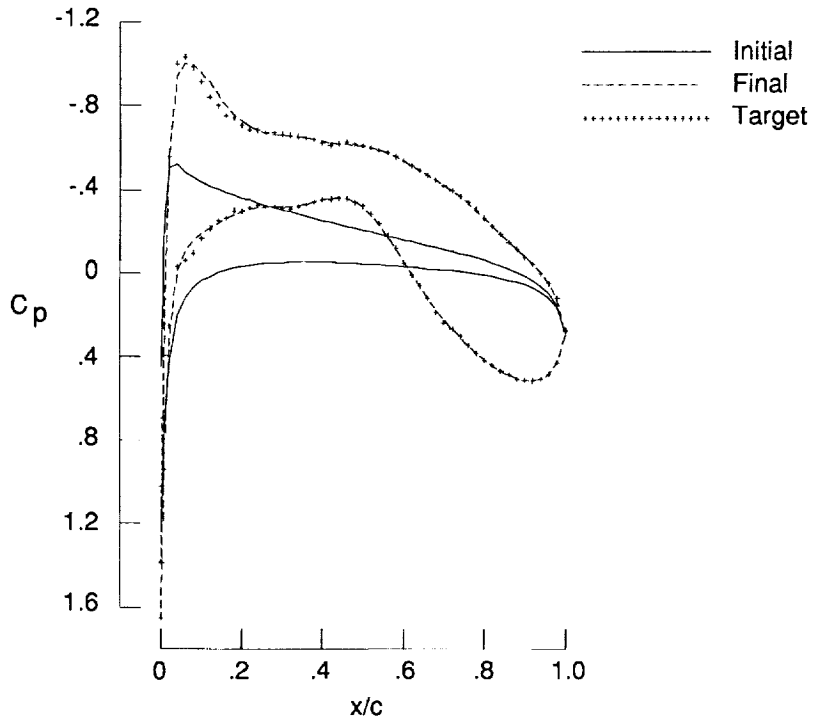

(a) Inboard; $\eta = 0.18$.

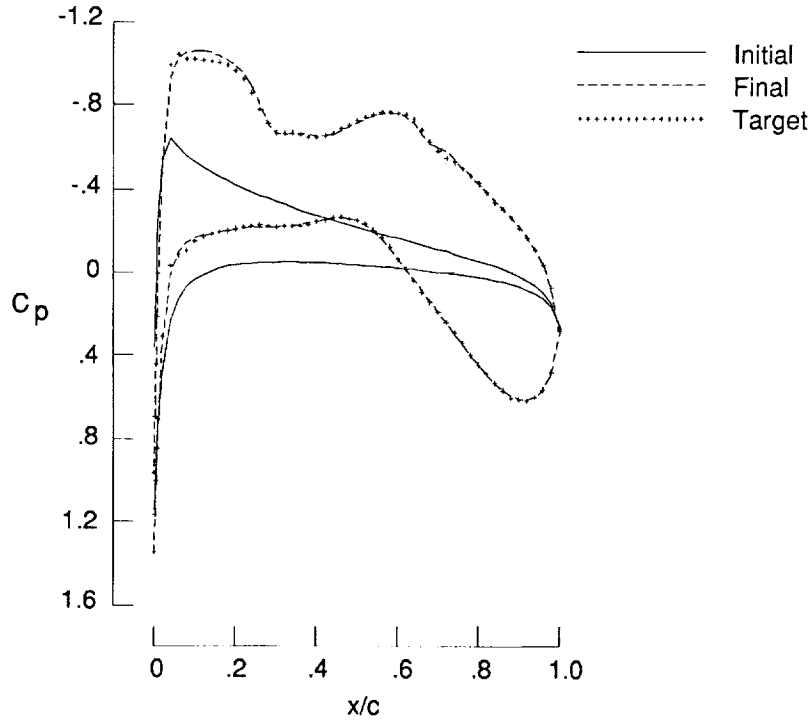

(b) Planform break; $\eta = 0.44$.

Figure 16. Pressure distributions for the automatic twisting case; $M = 0.80$, $\alpha = 1.0$.

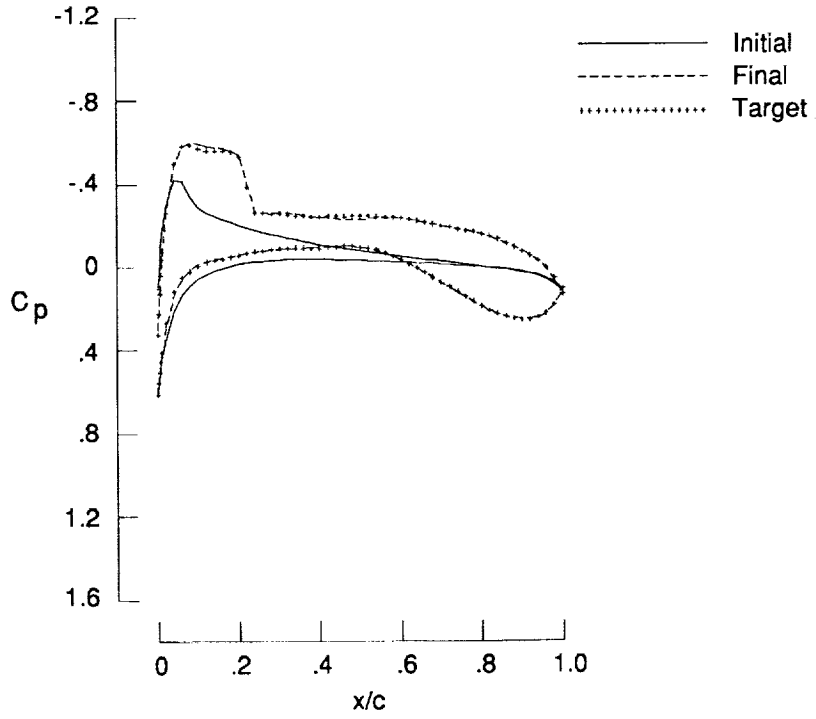

(c) Wingtip; $\eta = 1.0$.

Figure 16. Concluded.

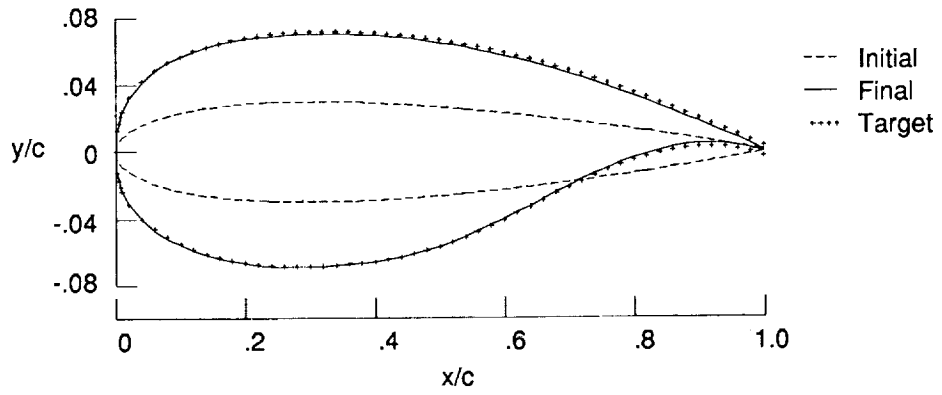

(a) Inboard; $\eta = 0.18$.

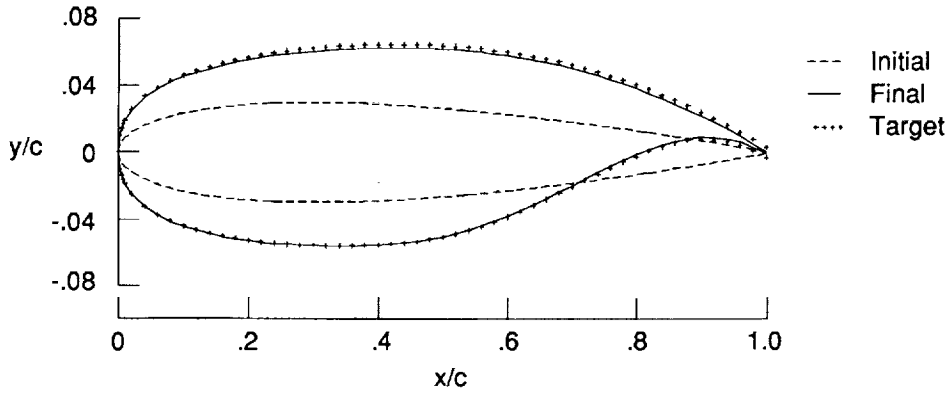

(b) Planform break; $\eta = 0.44$.

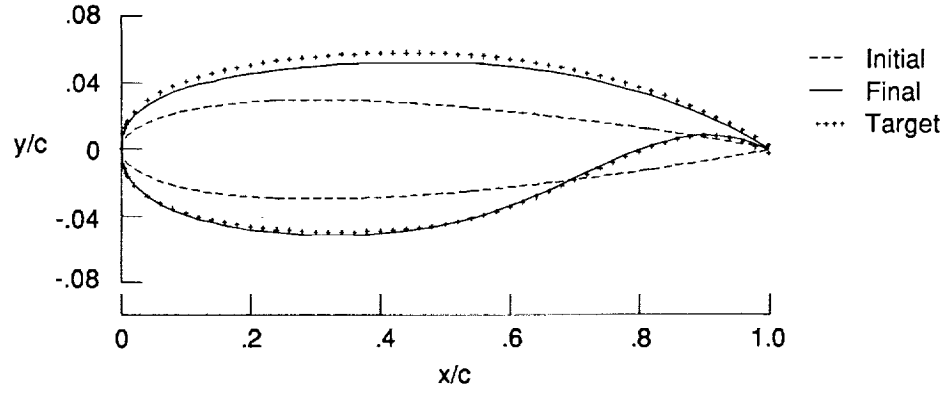

(c) Wingtip; $\eta = 1.0$.

Figure 17. Airfoil coordinates for the automatic twisting case; $M = 0.80$; $\alpha = 1.0$.

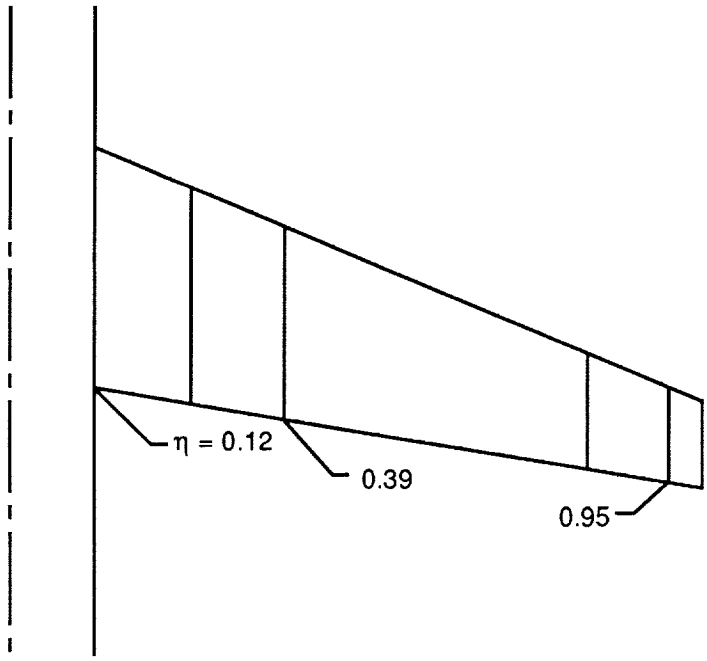

Figure 18. Planform shape for the applications case.

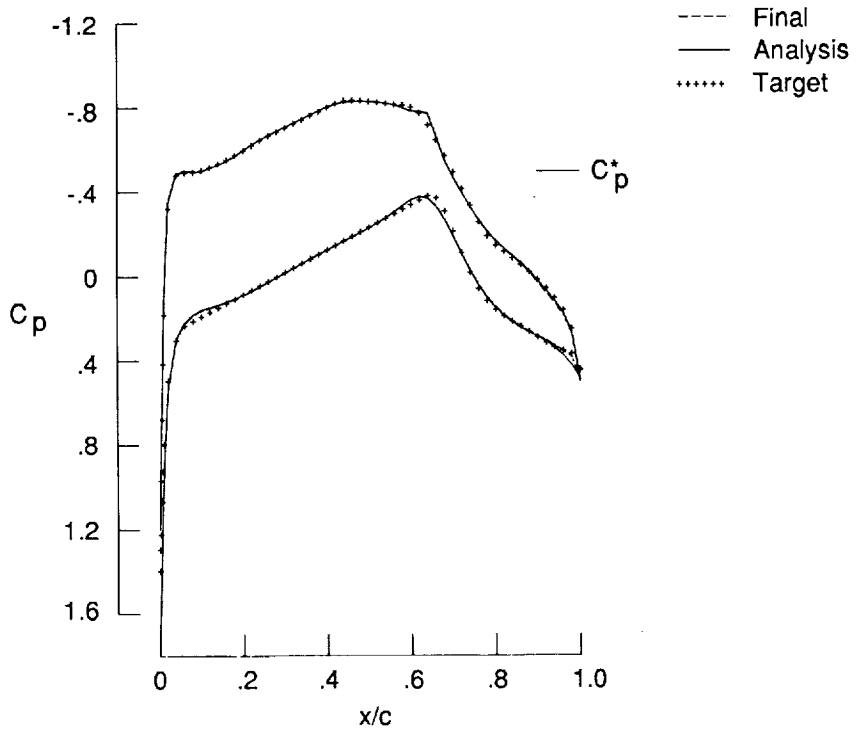

(a) Inboard; $\eta = 0.12$.

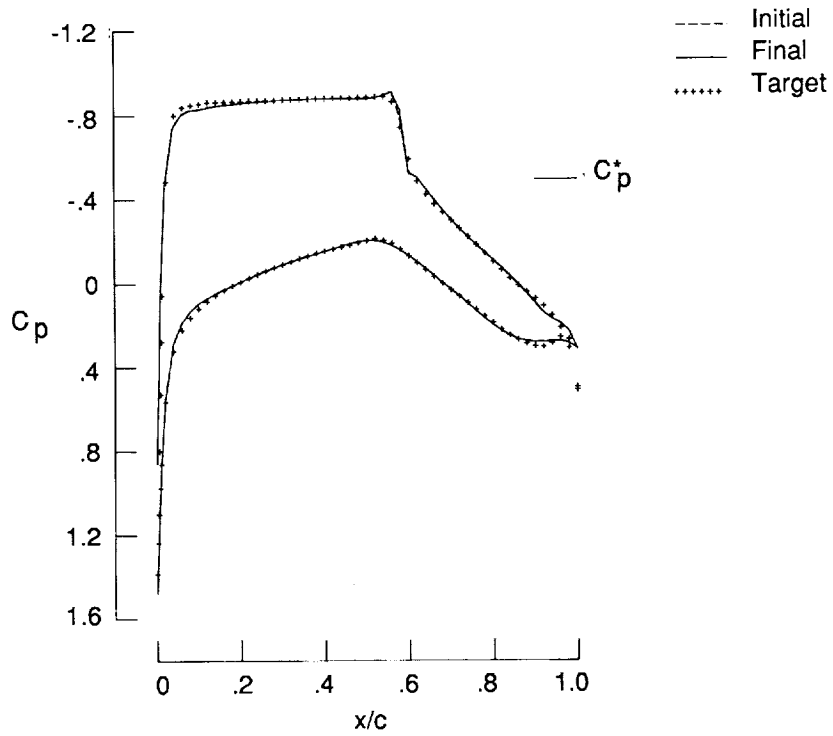

(b) Midspan; $\eta = 0.39$.

Figure 19. Pressure distributions for the applications case; $M = 0.78$, $\alpha = 6.1°$, $R = 8.35 \times 10^6$.

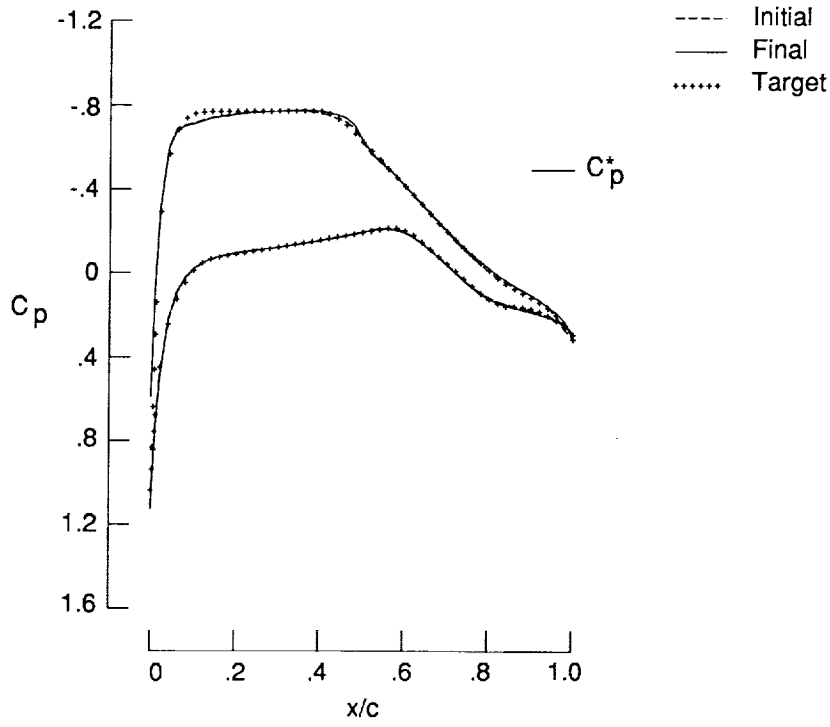

(c) Outboard; $\eta = 0.95$.

Figure 19. Concluded.

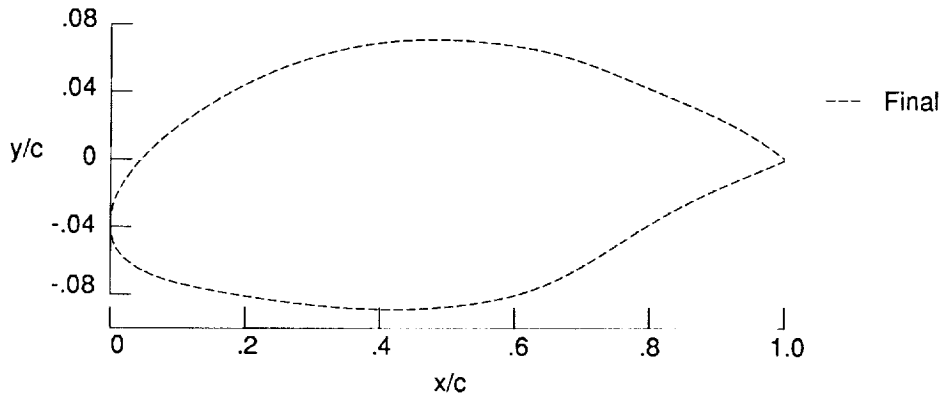

(a) Inboard; $\eta = 0.12$.

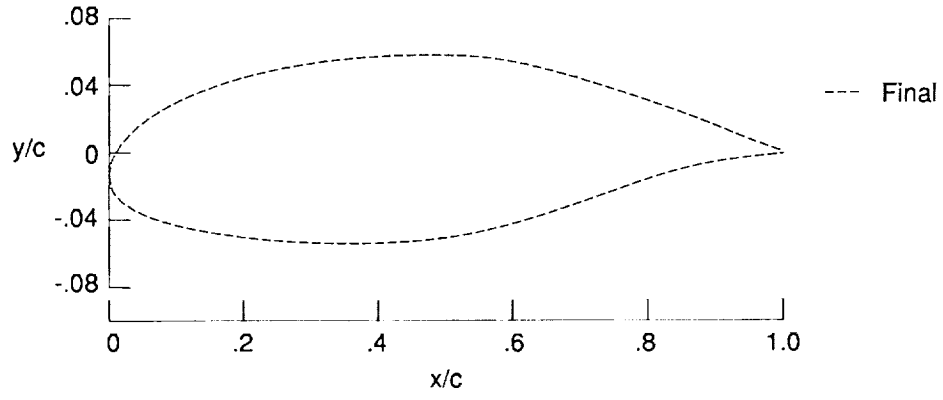

(b) Midspan; $\eta = 0.39$.

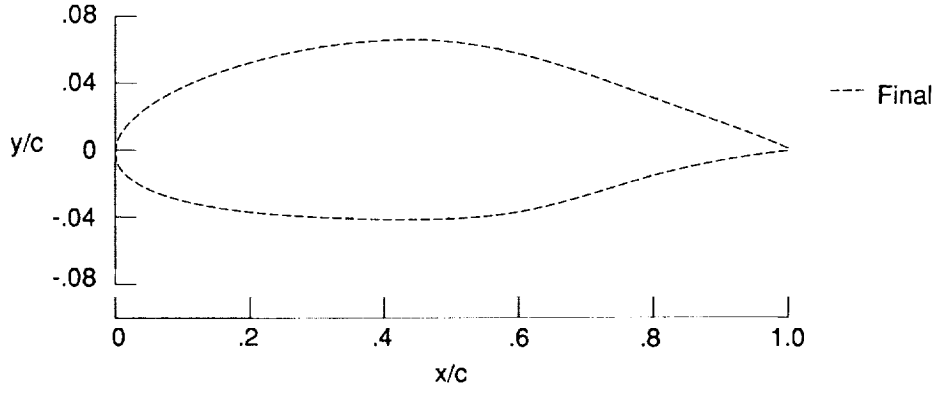

(c) Outboard; $\eta = 0.95$.

Figure 20. Airfoil coordinates for the applications case; $M = 0.78$, $\alpha = 6.1$; $R = 8.35 \times 10^6$.

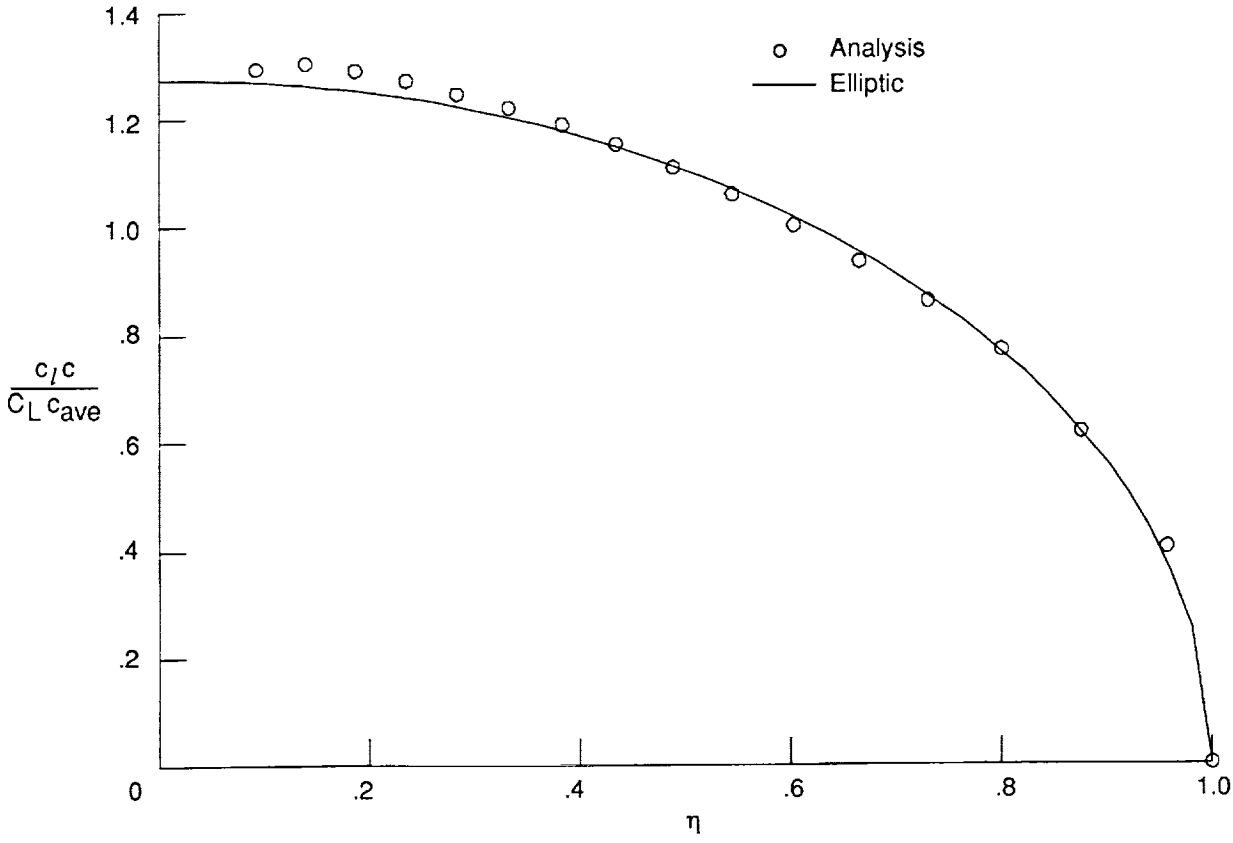

Figure 21. Span loading distribution for applications case; $M = 0.78$, $\alpha = 6.1$, $R = 8.35 \times 10^6$.

NASA
National Aeronautics and Space Administration

Report Documentation Page

1. Report No.	2. Government Accession No.	3. Recipient's Catalog No.
NASA TP-3045		

4. Title and Subtitle	5. Report Date
A Method for the Design of Transonic Flexible Wings	December 1990
	6. Performing Organization Code

7. Author(s)	8. Performing Organization Report No.
Leigh Ann Smith and Richard L. Campbell	L-16762

9. Performing Organization Name and Address	10. Work Unit No.
NASA Langley Research Center Hampton, VA 23665-5225	505-61-21-03
	11. Contract or Grant No.

12. Sponsoring Agency Name and Address	13. Type of Report and Period Covered
National Aeronautics and Space Administration Washington, DC 20546-0001	Technical Paper
	14. Sponsoring Agency Code

15. Supplementary Notes

16. Abstract

Methodology has been developed for designing transonic airfoils and wings; it includes a technique that can account for static aeroelastic deflections. This procedure is capable of designing either supercritical or more conventional airfoil sections. Methods for including viscous effects are also illustrated and are shown to give accurate results. The methodology developed is an interactive system containing three major parts. A design module has been developed that modifies airfoil sections to achieve a desired pressure distribution. This design module works in conjunction with an aerodynamic analysis module, which for this study is a small perturbation transonic flow code. Additionally, an aeroelastic module is included that determines the wing deformation due to the calculated aerodynamic loads. Because of the modular nature of the method, it can be easily coupled with any aerodynamic analysis code.

17. Key Words (Suggested by Authors(s))	18. Distribution Statement
Aircraft design Drag reduction Transport aircraft	Unclassified—Unlimited Subject Category 05

19. Security Classif. (of this report)	20. Security Classif. (of this page)	21. No. of Pages	22. Price
Unclassified	Unclassified	39	A03

NASA FORM 1626 OCT 86

NASA-Langley, 1990

For sale by the National Technical Information Service, Springfield, Virginia 22161-2171